Experiments in Heat Transfer Under Conditions of Oscillating Pressure and Flow

by

Peter D. L. Cheng

Bachelor of Science
University of California, Berkeley
(1993)

Submitted to the Department of Mechanical Engineering
in Partial Fulfillment of the Requirements for the Degree of

MASTER OF SCIENCE

at the

MASSACHUSETTS INSTITUTE OF TECHNOLOGY

May 1995

Signature of Author _____
Department of Mechanical Engineering
May 12, 1995

Certified by _____
Professor Joseph L. Smith, Jr.
Thesis Supervisor

Accepted by _____
Professor Ain A. Sonin
Chairman, Departmental Graduate Committee

Experiments in Heat Transfer Under Conditions of Oscillating both Pressure and Flow

by

Peter D.L. Cheng

Submitted to the Department of Mechanical Engineering on May 12, 1995,
in the partial fulfillment of the requirements for the degree of
Master of Science

Abstract

Correlations developed for steady pressure and flow to predict heat transfer are inadequate under conditions of oscillating both pressure and flow. This has been shown both theoretically and experimentally. Since almost every reciprocating energy conversion machine operates in an oscillating environment, and heat transfer has a significant effect on engine efficiency, it is imperative that mathematical correlations should be developed to predict heat loss through the walls of components within these systems.

A large heat transfer apparatus was built in 1990 to stimulate the oscillating environment found in Stirling engines. Later modifications to the apparatus allow more accurate measurements of velocity, pressure, centerline temperature, wall temperature, and heat flux. It is also capable of capturing temperature and velocity profiles across the diameter of the test section. This work addresses the collection of baseline data under conditions of oscillating pressure and flow by (a) investigating the disappearance of seeding particles at a certain part of the cycle, (b) continuing the experiment for a wider range of conditions, and (c) recording and analyzing baseline heat transfer data.

Results confirm that there exists a phase difference between centerline-wall temperature difference and heat flux. The results further show that the phase shift depends on both oscillating Pcelet number and compressor phase angle. Laser Doppler Velocimeter proves to be a valuable piece of instrument in an oscillating pressure and oscillating flow experiment.

Thesis Supervisor: Dr. Joseph L. Smith, Jr.
Title: Professors of Mechanical Engineering

Acknowledgment

During the past year working in Cryogenic Engineering Laboratory, I was able to learn a great deal outside school. It gave me a valuable experience of how working in society would be like, how to handle most problems on my own, how to take responsibility of the project given. To sum up, here is just like a miniature of the real world!

First, I would like to thank Prof. Joseph L. Smith Jr. for giving me the project. I also want to thank Prof. John Brisson. He has been offering all kinds of help in all the optical and electronics instruments. So have been Prof. John H. Lienhard V and Prof. Bora Mikic who were always trying their best whenever I talked to him to seek help. Also, I would like to thank Doris for proofreading my thesis.

Second, I would like to give my sincere thanks to the former person, William Grassmyer who worked on the project previously. He drove up here three times to show me how to run the experiment and he gave me much help on the phone as well.

Third, the technicians here have been very warm, kind and friendly. Bob Gertsen has been particularly friendly for his warmth, willingness to lend his hand and his guidance and technical advice. Mike Demaree was also giving much help whenever I reached him .

I also have to thank my friends at CEL. Paul Huang has given me sanity and social life in the laboratory. Beside my friends at CEL, there were also a number of friends of mine who constantly gave me supports. I would give many thanks to my friends at Berkeley, especially Linh Thai and James Lew. At MIT, Brandon Gordon, Hong-man Leung, Paul Ngan, Yurdun Orbak, KK Tang and, Steve Tang were also the ones I want to thank dearly.

I will also make use of the chance to thank NASA-Lewis Research Center and Oak Ridge National Laboratory for their support of the project.

Lastly and most importantly, my family. My parents gave me a very dear chance to study aboard and constantly showed their care about the progress of my work. Also, my brother Anthony, who is studying for Ph.D. in Cambridge, England sent me e-mails to confide and encourage me a lot. They have all been very supportive to me. Without them, I can hardly imagine what my life would have been like.

Table of Contents

List of Figures

Nomenclature

Variables

B	Angle of incidence of a seed particle striking probe volume
c_p	Specific heat at constant pressure
c_v	Specific heat at constant volume
d_f	Distance between two adjacent fringes in probe volume
d_m	Half width of probe volume
d_p	Particle diameter
D	Diameter of pipe
D_h	Hydraulic Diameter
D_{e-2}	Laser Beam diameter based upon e^{-2} intensity at front focusing lens
f	Frequency of compressors oscillations
h	Heat Transfer coefficient
i	Imaginary number = $\sqrt{-1}$
k	Thermal conductivity of gas
l_m	Length of probe volume
L	Length of the pipe between the compressors
n	n-th harmonic
Nu_c	Complex Nusselt number
Nu_i	Imaginary component of complex Nusselt number, Nu_c
Nu_r	Real component of complex Nusselt number, Nu_c
P	Pressure
Pe_ω	Oscillating flow Peclet number, $\omega \cdot D^2/\alpha$
q	Heat flux
q_c	complex heat flux
q_n	n-th harmonic of complex heat flux, q_c
r_p	Pressure ratio, (maximum pressure per cycle)/(minimum pressure per cycle)
r	Radius
Re	Reynolds number, $V_{max} \cdot D/\nu$
t	Time
T	Temperature
T_c	Centerline gas temperature
T_w	Wall temperature
U	Internal energy or velocity of flow inside a pipe
u_T	Thermophoretic velocity
v	Radial velocity component in a pipe
V	Volume
V_s	Terminal Rate of settling of a particle
α	Thermal diffusivity
δ	Stoke boundary layer thickness, $(2 \cdot \nu/\omega)^{1/2}$

ΔT	Temperature difference between centerline gas temperature, T_c and wall temperature, T_w
ΔT_n	n-th harmonic complex temperature difference, T_c
κ	Half angle between two incident laser beams
λ	Wavelength of laser beam or mean free path of gas molecules
ν	Kinematics viscosity
Φ	Phase of harmonic
ψ	Pfriem's variable
Ψ	Phase lead of driven compressor over undriven compressor
ρ	Density
ω	Angular frequency
ϑ	Precipitation efficiency

Subscripts

c	Complex, Centerline
i	Imaginary component
n	n-th harmonic
r	Real component

Chapter 1

Introduction

1.1 Background

A large portion of energy conversion equipment that is in use is reciprocating machinery with gas as the working fluid. In some devices such as the Stirling engine, the working space consisting of a simply shaped clearance volume over a piston in a cylinder, is closed. In calculating the performance of the thermodynamic cycles, the processes within a cylinder are often assumed to be adiabatic. In fact, there is always a certain amount of heat transfer between the gas and the cylinder wall. The heat transfer may be undesirable and significantly degrade the actual performance of the devices. Therefore, it is imperative that we understand the mechanism of heat transfer in such an environment. The objective of this work is an attempt to look for more accurate heat transfer correlations which can be then be used in the design of reciprocating engines.

The design of reciprocating engines has been based on extrapolation of expressions which were developed for the steady pressure and steady flow conditions. Both theories and experiments confirm that these expressions cannot correctly predict the performance of machinery which operates under the conditions of oscillating pressure and flow. Not only are the correlations incorrect, but also some of the parameters used in the correlations are not applicable to the oscillating pressure and flow conditions. This can be

understood from the fact that there always exists a phase shift between mixed-mean gas-to-wall temperature difference and heat transfer. The steady state correlations have no term to account for this phenomena.

In spite of the fact that these phase-shift phenomena were predicted analytically more than 50 years ago and demonstrated experimentally about 30 years ago, finding and use of correct correlations has not been a first priority. It is probably due to achievement of near-optimum designs from many years of trial and error. However, it is not a cost-effective way in view of high development costs for a new configuration. Study of the phenomena will allow clearer understanding of the heat transfer mechanism and the development of expressions for more accurate predictions of engine performance. There has been a revived interest in Stirling Engine because of its attractive features: quiet operation, non-polluting character, long life, high efficiencies for varying loads and high power density. An experimental apparatus has been built to facilitate the study of heat transfer under such conditions.

This thesis reports the continuing effort in attempting to predict correlations for heat transfer with an alpha-typed Stirling Engine simulated experimental apparatus. An alpha-typed Stirling engine uses two pistons which mutually compress the working gas in the cold space, move it to the hot space where it is expanded and then moved back; there is a regenerator and a heater and cooler in series with the hot and cold gas spaces. The apparatus is capable of measuring velocity, centerline temperature, wall temperature,

pressure, heat flux and crank angle over a wide range of experimental conditions. Since phase shift exists between heat flux and temperature fields, the results are expressed in terms of a complex-valued Nusselt number. The experimental results are correlated in that form.

1.2 Stirling Engines

1.2.1 A brief History

In 1816, the Reverend Robert Stirling had invented a hot-air engine even before thermodynamics was born. At that time, the engine satisfied the demand for a small power plant, for steam engines were impractical in the low-power range due mainly to excessive heat loss. However, steam engines became prominent again when the problem was minimized. Stirling engines seemed destined for oblivion.

Just before World War II, Philips Company of the Netherlands found that in view of the recent technological advances, it might be worthwhile to re-examine the hot-air engine. Furthermore, there was a substantial need for a small, simple power plant for radio transmitters and receivers. Thus, Philips started the development of the modern version of Stirling engines. New design was able to overcome old problems (low efficiency, inferior heat exchange rates) to achieve competitive levels of efficiency. Philips Company also discovered that if the cycle was reversed, it turned out to be a very efficient refrigeration plant. However, no theory of sufficient breadth and depth serving as the

basis for designing such an engine appeared to have been published in the open literature, albeit of the success in the production of the engines.

1.2.2 The Cycle

The Stirling engine is like any heat engine, it goes through the four basic processes: compression, heating, expansion, and cooling (Fig. 1.1).

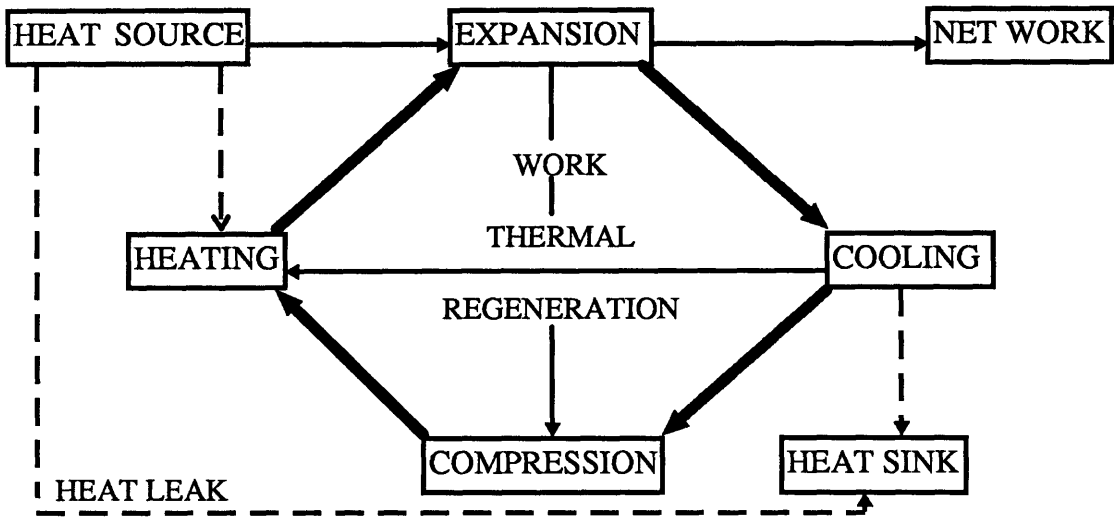

Figure 1.1 Common Process for all Heat Engines

The operation of an idealized Stirling engine is described as follows (Fig. 1.2).

(a) *Isothermal expansion process* (1 - 2)

The right piston now remains stationary as the left piston continues to move down while in contact with the hot reservoir, causing the gas to undergo an isothermal expansion, during which heat $|Q_H|$ is absorbed at the temperature θ_H. There is no change in the internal energy, but an increase in the entropy of the gas.

(b) *Constant-volume regenerative transfer process* (2 - 3)

Both pistons move in opposite directions in a constant volume process. In doing so, gas is forced through the regenerator from the hot to the cold side and gives up the same amount of heat $|Q_R|$ to the regenerator that is absorbed in (4 - 1). No net work is done, and there is a decrease in the internal energy and entropy of the gas.

(c) *Isothermal compression process* (3 - 4)

While the left piston remains at the top, the right piston moves halfway up, compressing cold gas while in contact with the cold reservoir and therefore causing heat $|Q_C|$ to leave. Work is done on the working fluid equal in magnitude to the heat rejected from the cycle. There is no change in internal energy, and there is a decrease in entropy.

(d) *Constant-volume regenerative transfer process* (4 - 1)

The left piston moves down and the right piston up so that there is no change in volume, but the gas is forced through the regenerator from the cold side to the hot side and enters the left-hand side at the higher temperature θ_H. To accomplish this, the regenerator supplied heat $|Q_R|$ to the gas. No net work is done, and there is an increase in the entropy, and internal energy, of the gas.

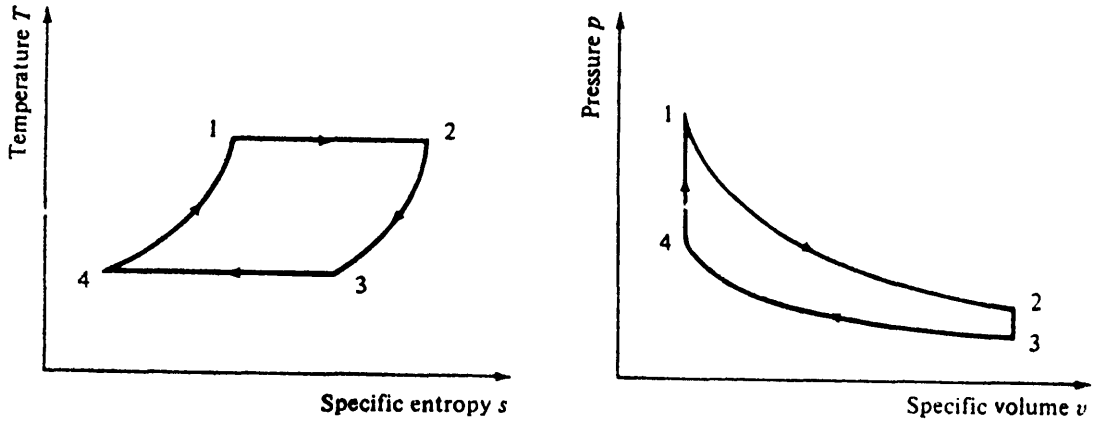

Figure 1.2 The Ideal Cycle of Stirling Engine

The assumptions for the idealized cycle is that (1) the gas is ideal, (2) no leakage of gas takes place, (3) no heat is lost or gained through the cylinder walls, (4) no heat is conducted through the regenerator, (5) there is no fiction, (6) no temperature difference between gas and TH or TL or T_{wall} in regenerator, and (7) no gas volume in the regenerator.

The above assumptions involve gross idealization of the process occurring in an actual Stirling engine. They are not realistic enough for actual engine design calculations. A more realistic description of the cycle called "The Schmidt Cycle" was done by Gustav Schmidt in 1871. The full analysis can be found in *Stirling Engines*, 1980 pp. 50-57 by G. Walker (28).

1.3 Demonstrations of Heat Transfer Phenomena

1.3.1 Experimental demonstration of Heat Transfer Phenomena

From the operation, we can see that the Stirling engine resembles other types of reciprocating engines working in an oscillatory environment.

In an actual Stirling engine, heat transfer through cylinder walls is not insignificant. During compression, work is done by the piston on the working fluid. The mixed-mean temperature of the working fluid increases and is above the wall temperature. Newton's law of cooling, which is a steady-state correlation, predicts a net heat transfer out of the fluid to the wall. However, the portion of fluid that is close to the cylinder wall has a

temperature close to that of the cylinder wall. Consequently, the heat transfer may not be as large as predicted by the law. Also, during initial expansion, the fluid expands at such a rate that it does not have enough time to settle itself to a steady-state profile. The portion of the fluid close to the cylinder wall will fall to a temperature below the cylinder-wall temperature and hence the net heat transfer will enter the fluid. Unfortunately, Newton's law predicts there should still be a net heat transfer out of the fluid since the mixed-mean temperature of the fluid remains higher than that of the cylinder wall. Worse still, there are occasions where there is no difference between mixed-mean temperature and wall temperature but a non-zero heat transfer. Thus, an infinite Nusselt number results. There is a breakdown of steady-state correlations when applied to unsteady conditions. Phase shift between temperature difference and heat transfer is inherent in oscillatory environment.

1.3.2 Theoretical demonstration of Heat Transfer Phenomena

One of the early investigations of heat transfer within an oscillating flow was conducted by H. Pfriem (22). He basically solved a simplified energy equation.

$$\frac{\partial T}{\partial t} = \alpha \frac{\partial^2 T}{\partial x^2} + \frac{1}{\rho c_p} \frac{\partial P}{\partial t} \tag{1.1}$$

In his analysis, he assumed that density was constant and the convection was negligible. His assumption of the constant density introduced error into his simplified solution on the order of c_P versus c_V. Nevertheless, he showed heat transfer under

conditions of oscillating pressure should be out of phase with the mixed mean temperature to wall temperature difference. His resulting complex Nusselt number equation is:

$$Nu_c = D \cdot \Psi \cdot \frac{\left[\left(1-e^{-2\delta\Psi}\right)+s\cdot\Psi\left(1+e^{-2\delta\Psi}\right)\right]}{\left[\left(1-e^{-\delta\Psi}\right)^2+s\cdot\Psi\left(1-e^{-2\delta\Psi}\right)\right]} \tag{1.2}$$

where,

$$\Psi = \sqrt{\frac{i\omega}{\alpha_0}}$$

$$\delta = \sqrt{\frac{2\nu}{\alpha_0}}$$

$$\delta = \frac{Volume\ of\ Turbulent\ Core}{Surface\ Area\ of\ Heat\ Transfer}$$

For low frequency oscillations, periodic heat flux and temperature difference are in phase whereas at high frequencies, the heat flux leads the temperature difference by 45°. Recently, a number of research groups have successfully demonstrated that Pfriem's analysis was generally representative of the phenomena of oscillating heat transfer.

In 1983, K.P. Lee (17), independently made an analytic study of heat transfer with a cyclic pressure variation by again solving 1-D energy equation, assuming negligible convection and density variation. Lee's equation for the complex Nusselt number is:

$$Nu_c = \sqrt{\frac{Pe_\omega}{2}} \cdot \frac{\left[(1+i)\tanh z\right]}{\left[1-\tanh z/z\right]} \tag{1.4}$$

where

$$z = (1+i)\cdot\sqrt{\frac{Pe_\omega}{32}}$$

$$Pe_{\omega} = \frac{\omega \cdot D^2}{\alpha}$$

Lee's results is in agreement with Pfriem's. There is no significant phase shift at small oscillating Peclet number, Pe_{ω} and the phase lead of heat transfer over the temperature difference does not exceed more than 45° at large Pe_{ω}.

1.4 Research Objectives

Although our main goal is to look for complex number corrleations of the heat transfer data, there have been some problems within the apparatus that needed to be resolved first before we can believe in the reliability of the data collected. As a result, the objectives of the research project were to:

- First, attempt to investigate the disappearance of seeding particles at a certain part of the cycle,
- Second, continue the research for a wider range of conditions,
- Third, collect baseline data at allowable range of frequencies of the apparatus and at phase angles: 0°, 45°, 90°, 135°, between the compressors.

Chapter 2

Experimental Apparatus

The apparatus has gone through several phases of modifications since it was built. Yung Ho (10) is credited for designing and building the heat transfer. Ho's (10) work is addressed as Phase 1 of the equipment's development. Later on, Alexander Tziranis (27) modified the apparatus by redesigning the test section. The modification was basically an addition of a heat flux gage and a traversing thermocouple to the test section so that measurement of the wall heat flux could be achieved. Tziranis's (27) work represented Phase 2 work. Phase 3 work on the apparatus was carried out by Charles Dean (3). He installed a Laser Doppler Velocimeter (LDV) in the apparatus with a traversing system. Velocity could then be obtained accurately avoiding the lengthy inaccurate velocity calculations required before. Most of the ground work for optimizing the system was done in Phase 1-3. William Grassmyer (8) carried out some minor modifications to optimize the apparatus further. He reduced the noise level originating from the laser power supply by covering it with an aluminum foil wrapped box. He was also responsible for developing data reduction software.

2.1 Phase 1: Birth of Ho-Smith's Heat Transfer Apparatus

In order to study further on the heat transfer under the conditions of oscillating pressure and flow found in Stirling engine, Yung Ho (10) under Professor Joseph L.

Smith, Jr.'s supervision in the Cryogenic Engineering Laboratory at MIT, designed and built a dual compressor experimental apparatus to simulate the working environment of an alpha-typed Stirling engine (Fig. 2.1).

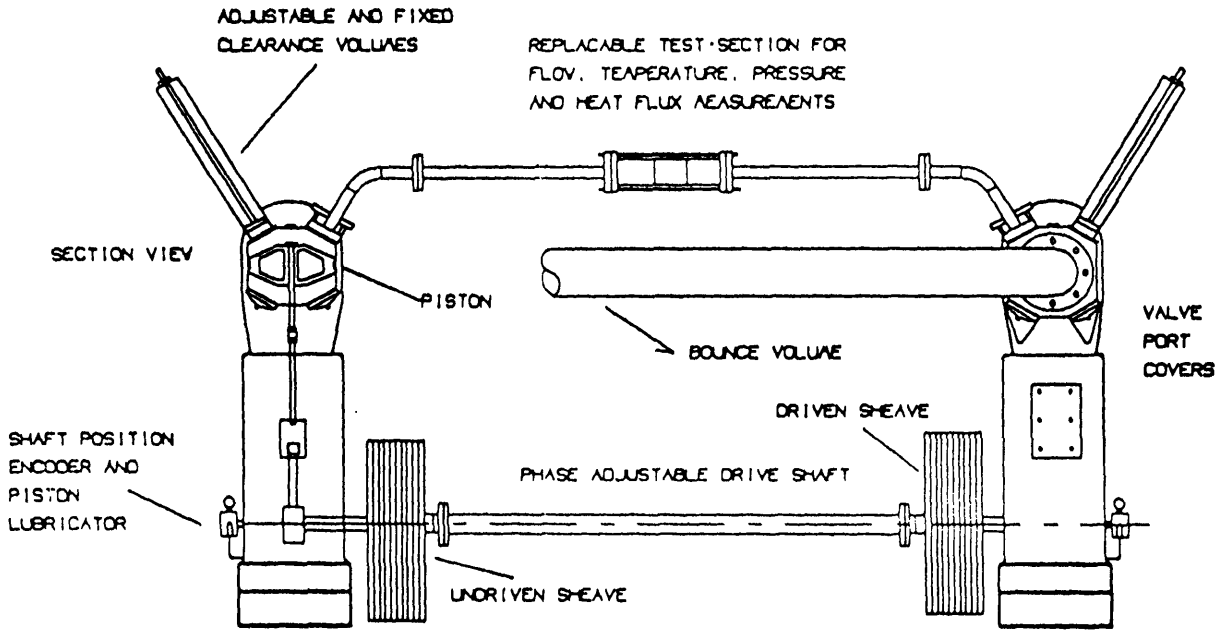

Figure 2.1 The Schematic of the Experimental Setup (10)

The apparatus is mainly made up of six elements: two 9-inch stroke by 11-inch bore JOY compressors joined by a common drive shaft and with a variable phase angle Ψ between the two compressors, a Westinghouse 25 HP DC motor that powers the outlet/inlet ports on the head of each compressor, a three-piece 1.75-inch diameter test section centered in the middle of the pipe connecting these two compressors, two variable clearance volumes mounted to the head of each compressor to enable adjustments of the pressure ratio within the test section, and a bounce volume pipe connecting the piston in one compressor to the

gas occupying the same space in the other compressor. The DC motor controls the RPM of the compressor crankshaft by varying the voltage of the auto transformer. The compressor which is connected to the motor directly is the driven compressor and the other is the undriven compressor.

The apparatus was capable of measuring gas pressure, wall temperature, and the crank angle of the undriven compressor, but the wall heat flux and the flow velocities had to be calculated from the recorded data.

Ho (10) modified Kornhauser's (12) earlier data acquisition program so as to collect data from two eight channel Data Translation DT2801-A analog and digital I/O boards. Data collection was triggered by a Vernitech optical shaft encoder mounted to the undriven compressor crank shaft. Ho also wrote a data reduction program and a data analysis program. They can be found in his 1991 thesis.

2.2 Phase 2: A traversing Thermocouple System and a Wall Heat Flux Sensor

During 1990-1991, Alexander Tziranis (27) took over and continued the project. He made several changes to the apparatus. The test section was modified and additional instrumentation was installed. The 5.5-inch extension rod for a traversing thermocouple passed through a drilled and threaded hole in the wall. A conical hole through the wall served as an optical view window for a LDV system. A heat flux sensor was mounted on

the inside of the Pyrex glass pipe which lined the test section. A traversing system for the thermocouple was constructed and installed. The traversing thermocouple system measured the gas temperature distribution across the test section as shown in Figure 2.2.

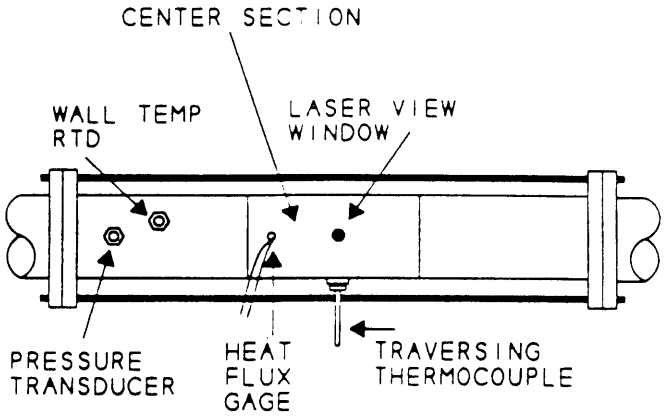

Figure 2.2 The Test Section of the apparatus (3)

The traversing thermocouple was manufactured by the Paul Beckman Company. It is made up of a Type E thermocouple at the end of 0.008-inch diameter, 0.5-inch long hollow rod mounted to the end of a 0.125-inch diameter, 5.5-inch long stainless steel extension rod. The 0.008-inch rod separating the thermocouple junction from the 0.0125-inch extension rod was designed to minimize flow disturbances. The base of the thermocouple probe was mounted to a Berg model LBSC-20 ball slide. The slide is moved by a Hurst model 4014-002 Linear Stepping Actuator. The model 20455-1 heat flux sensor was made by RdF Corporation. The whole traversing system was mounted to the test section by bolting it to a flat section milled into the bottom to the test section.

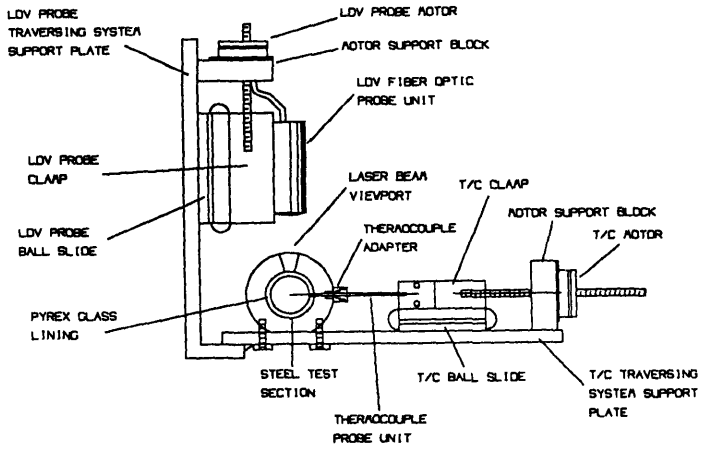

Figure 2.3 Tziranis's Thermocouple Traversing System (27)

2.3 Phase 3: Installation of a Laser Doppler Velocimeter System

Charles Dean (3), working on the project from 1992-1993, took the capability of the apparatus a big leap further by installing a Laser Doppler Velocimeter (LDV). The laser system and its accompanying software and hardware allow measurement of temperature and flow velocity data across the inside diameter of the test section, wall temperature and pressure, and compressor positions. The main use of LDV is that it can measure velocity across the inside diameter of the test section and replaces the inaccurate calculations for bulk velocity.

The Aerometrics laser system consists of a 300mW Omnichrome power supply for the Argon ion laser, a fiber drive, a photodetector, a digital signal analyzer (DSA) and a transceiver. A reference laser beam first enters the fiber drive after reflecting from the external mirrors along its path. Within the fiber drive, it passes through a filter which only

permits the 514 nm wavelength green light to go through and into the Bragg cell. While the software and hardware are on, the Bragg cell splits the reference laser beam into two beams with one of them at a frequency 40 MHz higher. The two beams strike the prismatic rhomboid and fiber optic cables after reflections from the internal mirrors inside the fiber drive. Both beams exit out from the transceiver and intersect at a distance 250 mm in front of the transceiver. Light scattered due to moving seed particles is reflected back through the transceiver and fiber optic cable. The scattered light then enters the photodetector where it is transformed into the voltage signal. The signal is then registered and processed by DSA to determine the velocity.

The laser traversing system was built to support and position the transceiver on top of the test section. It also included a stepping motor to facilitate measurements across the inside diameter of the test section. For further details on the traversing system, the reader is referred to Dean's thesis.

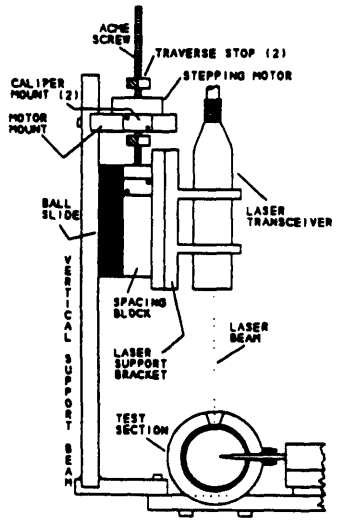

Figure 2.4 Experimental Setup of Phase 3 (3)

2.4 Phase 4: Noise Reduction and New Software Development

During Phase 3 of the experiment, there was an unexpected noise problem in most of the instrumentation. William Grassmyer (8), working on the project at the time, discovered that one of the main noise problems was 60 Hz noise. From his collected data, he discovered a huge number of noise spikes appeared in his graphs. The noise level was then minimized by installing a 192 Hz RC low pass filter. However, noise coming out from the Omnichrome power supply contributed another source of noise problem. The noise was fatally mistaken as the velocity data by the LDV's signal processor. Placing the power supply as far away as possible and covering it with an Aluminum foil wrapped box minimized the noise to a certain extent.

After the noise problem, Grassmyer (8) also worked on developing a new data reduction software. It is capable of smoothing and averaging the data and decomposing the data into the harmonics with a discrete Fourier Transform. The harmonically decomposed data can then be fed to another program to calculate the real and imaginary components of Nusselt number, and the phase shift between heat flux and gas-wall temperature difference.

A list of the programs can be found in Appendix A.

2.5 Instrumentation for the Heat Transfer Apparatus

There are a total of six sensors placing around the test section for measurement.

(1) Pressure: A Kulite model XT-190 strain gage transducer was used for pressure measurement. The range of the transducer is from 0 to 500 psi. Since pressure was assumed to be constant throughout the test section, the sensor could be mounted at any position along the test section.

(2) Wall Temperature: A Medthem model PTF-100-20404 resistance temperature detector (RTD) was used for wall temperature. The gage was mounted slightly off center but the error was found to be negligible.

(3) Centerline temperature: A Type E fast-response thermocouple custom made by the Paul Beckman Company was used to measure centerline temperature. The main body of the probe is housed inside a 0.125 inch, 5.5 inch long stainless steel cone. The micro-disc thermocouple junction is located on the end of a 0.1 inch long 3 mil diameter quartz sheath housed inside an 8 mil diameter stainless steel tube. The thermocouple was attached to a traversing unit which allows for a temperature profile of flow to be taken.

(4) Crank and phase angle between Compressors: The crank angle readings were registered with a Vernitech Model VOE-023 optical encoder. The encoder pulsed 1200 times for each revolution with a reset at the end of each cycle. The encoder was located on the side with the DC motor. The phase angle between compressors was set by first rotating the undriven piston to bottom dead center. Once both pistons were at the bottom dead center, the driven piston was then rotated to the desired phase by counting the number of encoder pulses. Each encoder count corresponds to 0.3°.

(5) Wall Heat Flux: heat flux was measured by RdF Corporation model 20455-1 heat flux sensor. This sensor gave a direct measurement of heat flux through the walls. The sensor consists of two thermocouples sandwiching an 0.0005 inch substrate. The heat flux can be directly calculated from the voltage difference of the two thermocouples. The sensor was found to have a response of at least 8.0 Hz with a manufactured specified response of 50 Hz. The signal from the heat flux gage was amplified 10,000 times by cascading two 100-gain amplifiers. The first amplifier was an Analog Device 288J which was used to control the DC offset. The amplified signal was then filtered by a 192 Hz RC low pass filter and fed into an Analog Device AD624 precision amplifier.

(6) Velocity: Velocity measurements were taken with the Aerometrics Laser Doppler Velocimeter (LDV). Its general usage has been discussed in the Phase 3 development. Further explanation of the use of LDV will be discussed in the next chapter. The LDV transceiver is fastened on a traversing system which allows velocity profiles of the flow to be taken.

Chapter 3

Laser Doppler Velocimetry

Nowadays, the laser is an extremely popular tool in all sorts of measurement applications. One of the most widely used applications is found in velocity measurement in fluid flow. The laser is particularly useful to researchers in this area mainly due to its non obstructive nature of measurement. Other measurement techniques for fluid flow such as pitot tube, turbine meter, etc. have their limitations and drawbacks because each unavoidably lies within its own wake whenever the flow reverses. As a result, accurate measurement is not possible. Hot-wire anemometer is not suitable even though it is capable of responding to the rapidly fluctuating velocities. The hot-film anemometer is susceptible to probe interference and does not discriminate between flow directions. In addition, the hot-film anemometer will respond directly to the very large pressure and temperature oscillations present in the measurements. Laser measurement techniques are ahead of other techniques because of their ease of use and preciseness. This technique is also powerful in regards to its capability of working in either 1-D, or 2-D, or 3-D flow fields. In general, principles of laser measurement technique are similar in most Laser Doppler Velocimetry systems, and the following description on its functionality suffices to give anyone a general idea of how to work with such a piece of equipment.

3.1 Aerometrics Laser Doppler Velocimeter System

In chapter 2, there has been a brief introduction to the operation of the Laser Doppler Velocimeter. In this chapter, we will describe the functions of each piece of the system in more detail.

3.2 External Mirrors

The external steering mirrors direct and guide the reference beam from the output of the laser generator into the fiber drive. For optimum performance, the laser beam diameter entering the fiber drive must be between 1.0 mm and 1.5 mm. The top screws allow the beam to be tilted or moved up and down as a whole by turning either one or both respectively. Likewise, the bottom two screws on the external mirrors allow lateral tilting or displacement of the beam. Accurate and careful steering of the beam with these screws is necessary for aligning the laser system properly.

3.3 Fiber Drive

As the reference beam leaves the mirrors and enters into the fiber drive, it passes through two ports. The first port that the beam passes has a filter which separates all wavelengths but the 514 nm green light. The power of the laser beam is about 100 mW after passing through the ports. The function of the second port is to help orient the beam correctly when it strikes the Bragg cells.

3.3.1 Bragg Cells

When the reference laser beam, out from the air-cooled 300 mW Argon ion laser generator, enters the fiber drive, it goes through two ports before striking the hole of an acousto-optic modulator or the Bragg cell. Inside the cell, the beam is split into two of equal intensity. It is important to note here that the software and hardware should be on at that time; otherwise, only one beam is observed to strike the rhomboid. One of the beams called the first order beam has its frequency shifted higher by 40 MHz. The zero order beam remains unchanged in frequency. The frequency difference between the original beam and the shifted beam is due to the frequency of the acoustic waves generated by a piezoelectric transducer travelling within the cell at a speed V.

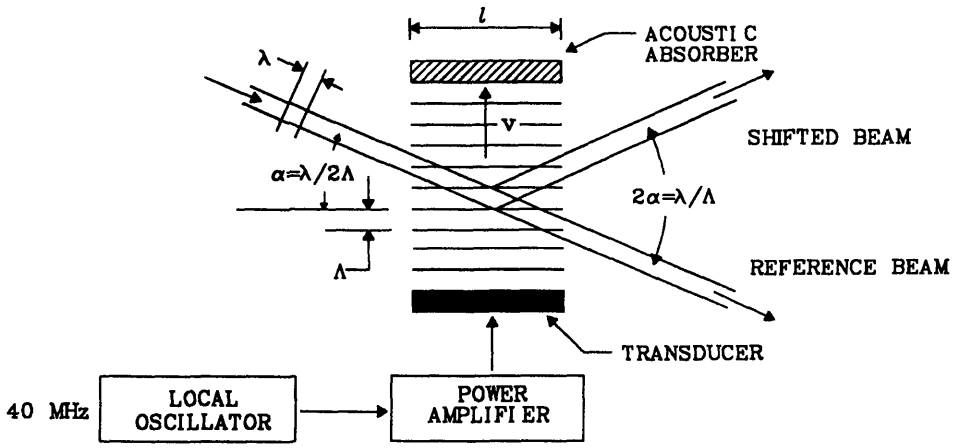

Figure 3.1 Beam Split and Frequency Shift inside Bragg Cell (TSI, 1992)

3.3.2 Rhomboid and Fiber Optic Couplers

Each laser beam coming out of the Bragg cell is reflected by the internal mirors and then strikes one of the faces of the rhomboid. The rhomboid then separates and

directs the beams to the couplers. Each coupler has two knobs attached on the side and two lenses inside. The pair of knobs on each coupler enable two-dimensional adjustments of the lens position. The knobs are adjusted so that the intensity and the power of each beam can be adjusted to maximum. At the same time, the knobs should be adjusted so that the power of one beam is close to that of the other. There is also a silver knurled nut on each coupler that joins a yellow optical fiber. The nut can be loosened. Within the nut, there is a silver cylinder which can be turned to position the polarization of the beam.

3.3.3 The Transceiver

Upon leaving the couplers, the beams then travels to the transceiver via a optical cable. The 50 mm fiber optic transceiver probe is an optical system that contains both transmitting and receiving components in a single package. It uses a series of optical fibers and lenses to transmit laser light. A transmitting lens is housed inside to focus and cross the beams in front of the transceiver. The volume formed by the intersecting beams defines the measurement volume of the probe called the probe volume.

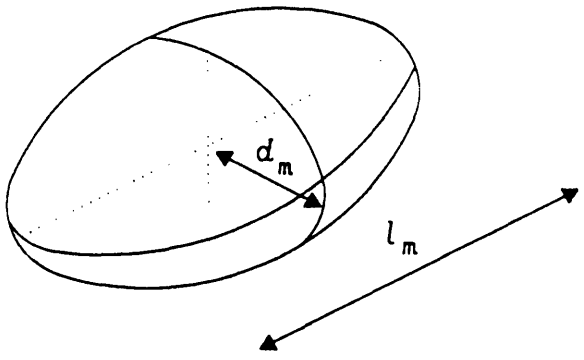

Figure 3.2 Probe Volume

(3.1) $$d_f = \frac{\lambda}{2\sin\kappa}$$ (spacing of fringes)

(3.2) $$d_m = \frac{4F\lambda}{\pi D_{e^{-2}}}$$ (width of probe volume)

(3.3) $$l_m = \frac{d_m}{\tan\kappa}$$ (length of probe volume)

where, F = the focal length of the transmitting lens

$D_{e^{-2}}$ = the diameter of the focused beam

λ = the wavelength of the laser

κ = the half-angle between the beams

The transceiver is connected to photodetector unit for the processing of light scattered from seed particles.

3.3.4 Seeding Particles

The important factor in the ability of the laser to measure the velocity of a flow field is the presence of seeding particles. The particles, preferably of size on the order of 0.1 to 2 μm in diameter, are used to seed the flow. They are moving at the same velocity as the flow. When a particle happens to enter the ellipsoidal shaped probe volume, the fringes within the volume is disturbed. It causes a modulation of light intensity at a frequency of:

(3.4) $$f_p = \frac{2u \cdot \cos(B) \cdot \sin\left(\alpha/2\right)}{\lambda}$$

where, B = angle of incidence of a seed particle striking the probe volume,
α = the angle between the beams
u = particle velocity.

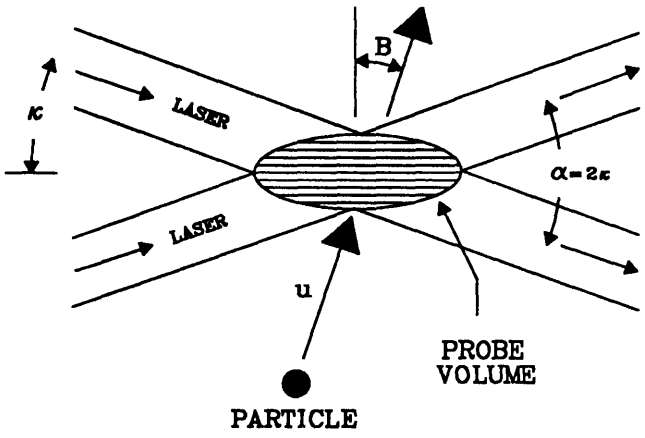

Figure 3.3 Interference of Fringe Patten

The light scattered by this particle is collected back through the same optical lens in the transceiver and picked up by a photodetector. The photodetector transforms the optical signal into the electrical equivalence. The signal is passed to signal processing software which determines the velocity u of the particle from the frequency of the reflected light:

$$u = \frac{d_f}{t} = d_f \cdot f_p \tag{3.5}$$

where t is the time to cross two adjacent fringes and f_p is the Doppler shift frequency of the light scattered by the particle.

The way that LDV is able to measure both positive and negative velocities can be understood as follows. In an oscillating flow environment, a particle's frequency differs based upon whether the particle is moving in the direction of the fringes in the probe volume or not. If it is moving in the same direction as that of fringes, it will have a frequency equal to f_p-f_{shift}. If it is moving in the opposite direction, it will have a frequency of f_p+f_{shift}.

3.3.5 Doppler Signal Analyzer (DSA) System

The DSA system is composed of several components: DSA's electronics, a high speed array processor, a computer interface card, and its own software. The DSA system analyzes and processes the signals received from the photodetector in a frequency domain. It can process Doppler frequency up to 150 MHz. A Fast Fourier Transform (FFT) algorithm is used to estimate the frequency of a sample. A Fourier Transform Burst Detector (FTBD) is loaded when acquiring data to help detect and concentrate the signal processing on the center of the burst to minimize noise processing.

Chapter 4
Seeding Methods

As mentioned in the last chapter, the flow field must be seeded before the laser can register or "see" signals from the particles and therefore determine the quantities (pressure, heat flux, centerline temperature and wall temperature) of the flow. There have been several seeding techniques.

4.1 Oil Smoke Generator

Much thought was given on how the test section could be seeded during Phase 3. Mineral oil smoke drops were chosen to be the seeding particles. The rationale for this choice is that mineral oil has a low vapor pressure. As a result of the low vapor pressure, the fine liquid droplets were assumed not to evaporate easily in the oscillating environment. Besides, the liquid drops are non-corrosive, have a non-clouding character and a size that is ideal to the specification of the seeding particles.

Seeding was done by pumping mineral oil by the Venturi effect into the burn chamber. The oil was heated and the droplets that were generated were then injected to saturate the whole test section. The entire setup for seeding is depicted in Fig. 4.1.

This seeding method proved to be ineffective because the oil droplets unexpectedly evaporated at the high pressure part of the cycle. Thus, the laser was unable to detect any droplets passing through the probe volume. Data could only be taken at the low pressure

part of the cycle. This phenomenon has been investigated for its cause at some length. But not much of it could be uncovered or explained at this time. In the end, alternative seeding method was deemed necessary.

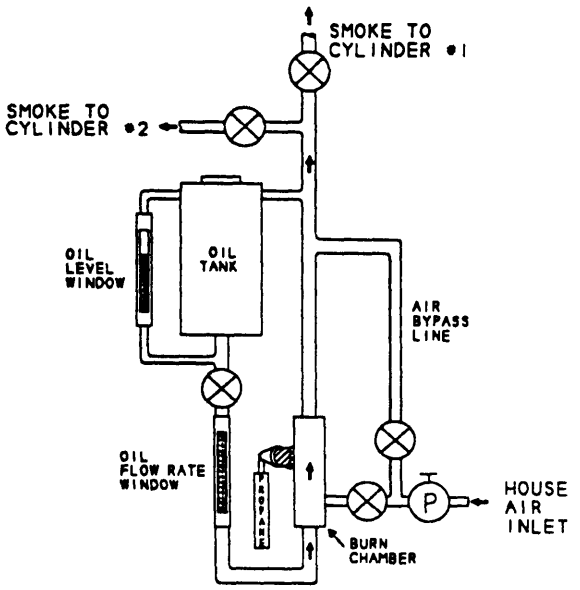

Figure 4.1 Mineral Oil Smoke Generator (3)

4.2 Alcohol Talcum Atomizer

Since there was a problem with fluid seed particles (mineral oil and propylene glycol), a new radical approach to seeding was proposed during Phase 4. Solid seed particles were tried instead of the previous "obvious" choices. The idea was to look for a solid substance which could be suspended in a volatile solvent. When the solvent evaporated, the solid particles would be floating in the flow field. Talcum powder was used because of its suitable size and its ease of suspension in alcohol. The alcohol would

evaporate quickly, leaving the Talcum powder floating in the test section. The setup used to perform the task is depicted in Fig. 4.2.

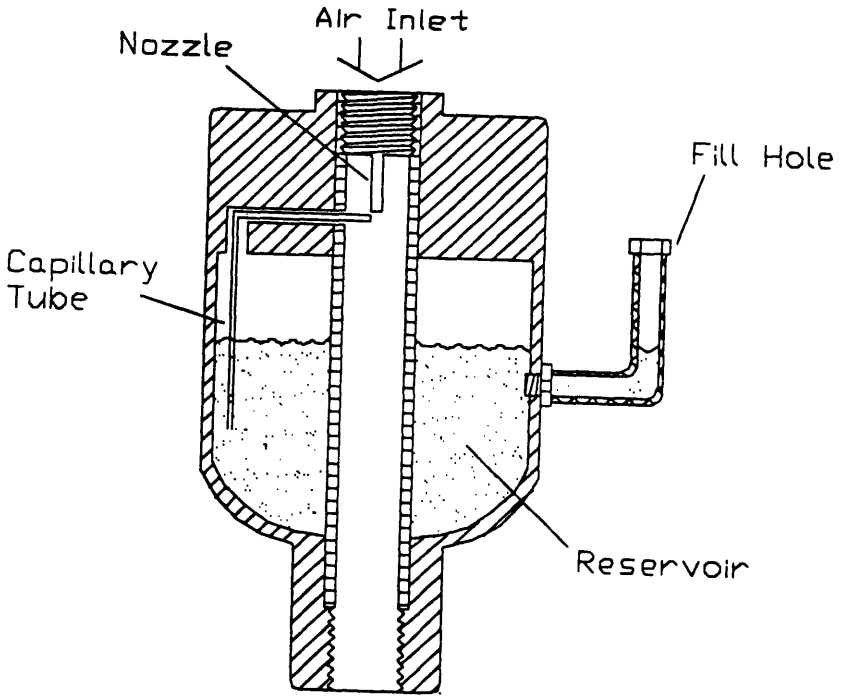

Figure 4.2 Alcohol-Talcum powder Atomizer (8)

Compressed air was blown through the nozzle so that the Talcum-alcohol mixture was then sucked up through the capillary tube by Venturi effect. The atomized mixture was injected into the test section.

The seeding method was once again not very successful though it was a very sound idea. The condensation of alcohol at the low pressure part of the cycle somehow blurred the visibility of the Talcum powder and hence velocity of that part of the cycle could not be measured.

4.3 Direct Injection of Talcum Powder

After a long investigation, a conclusion was that the evaporation effect was unavoidable if any form of liquid was injected into the system. The higher the vapor pressure, the greater the effect. As a consequence, only Talcum powder was injected into the test section. A funnel was filled with Talcum powder. There was a fine grain filter placed above the narrow opening of the funnel to only allow selected size of powder to be sucked into the test section. The seeding valve was closed off after a few cycles of suction. Disappearance of seed particles still occurred at the high pressure part of the cycle. Although further investigation is needed, use of highly reflected solid particles seems promising.

4.4 Possibilities to Alternatives of Seeding Particles

An investigation of the phenomenon has been launched in the hope that the mysterious problem of the disappearance of the seeding could be solved. After reviewing several descriptions of the phenomenon by many researchers and the trials of many different types of seeding particles and the ways to seed the flow, the general conclusion was; whenever the seeding particles are discharged into the flow, there always seems to be a disappearance of seeding particles in the working fluid. Moreover, it occurs with all types of seeding particles that were tried, although to different extents. The search for a more suitable type of solid particles, which we once thought promising, did not lead to a solution of the seeding problem. It was deemed necessary to carry out a much more careful investigation of the mechanism underlying the seeding problem.

4.5 An Investigation into the Disappearance of Seeding Particles

A new approach to the problem has been tried by reversing the phase angle between the compressors. Before, all experiments were carried out in such a way that the phase angle of the driven compressor always led that of the undriven compressor. By reversing the phase angle, we would like to investigate if the roles were exchanged. Previously, the particles were seen during the low pressure part of the cycle as the air moved out of the driven compressor. With the phase angle reversed, the particles would be seen at a different part of the cycle.

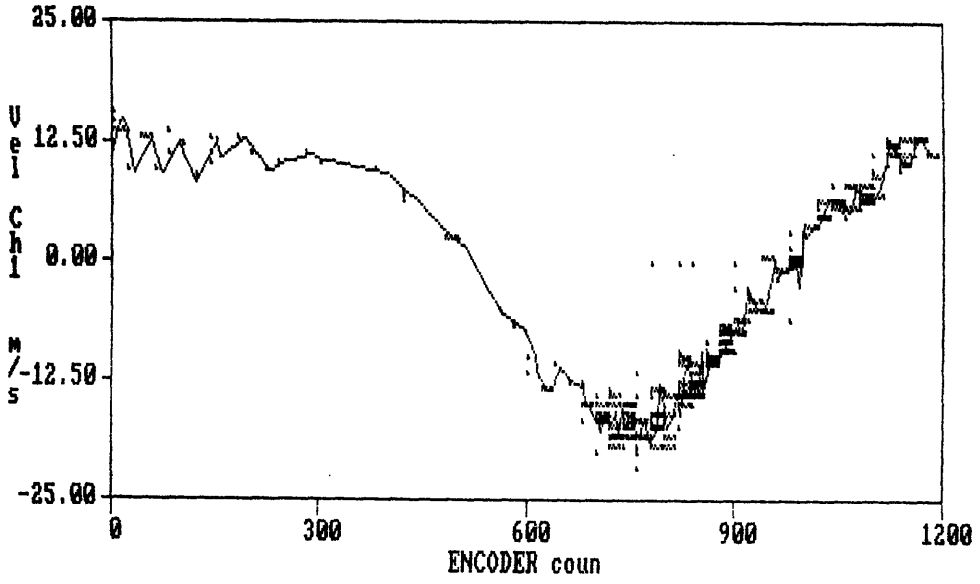

Figure 4.3 Velocity data taken at +90° compressor phase angle for a full cycle

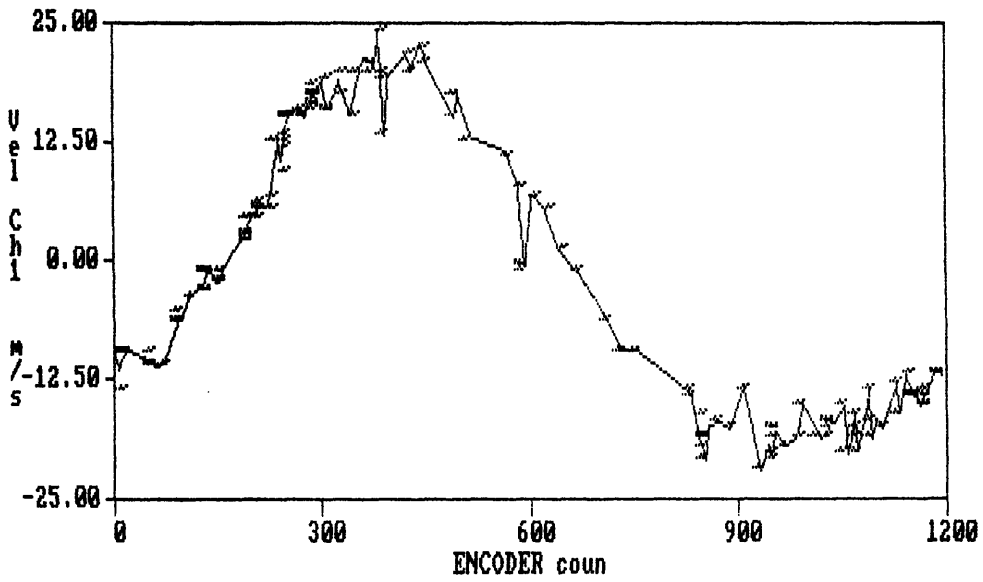

Figure 4.4 Velocity data taken at -90° compressor phase angle for a full cycle

As shown on the graphs above, one measurement was performed at phase angle +90° as previous runs and the other was at phase angle -90°. It is obvious that the first graph has most of the data points shown at a certain part of the cycle while the second one has a more or less evenly distribution of data points. From above, we may suspect that the disappearance of seeding particles is due to the asymmetry of the apparatus when it was first built. It may be likely that as the asymmetry is found, the mystery that has been recurring would be solved.

4.6 A Check of Leakage in Compressors

In order to investigate the asymmetry, the compressors were first checked to determine if they were to the problem. The test elbow section of each compressor was first detached from the test section. The opening of the test elbow was closed off with a plastic plate and See-shaped clamps. Sealing compound was applied to make certain that there was no possibility for gas to escape. Then, the pressure transducer was removed from the test section and inserted into the top of the compressor. Data was then taken and graphs were plotted.

The pressure graphs of each compressor show very smooth curves. There is not any sign of significant leakage. Furthermore, the pressure ratio determined to be 1.8 is close to the supposed value of 2.0. Therefore, it was concluded that the disappearance was still unaccounted for.

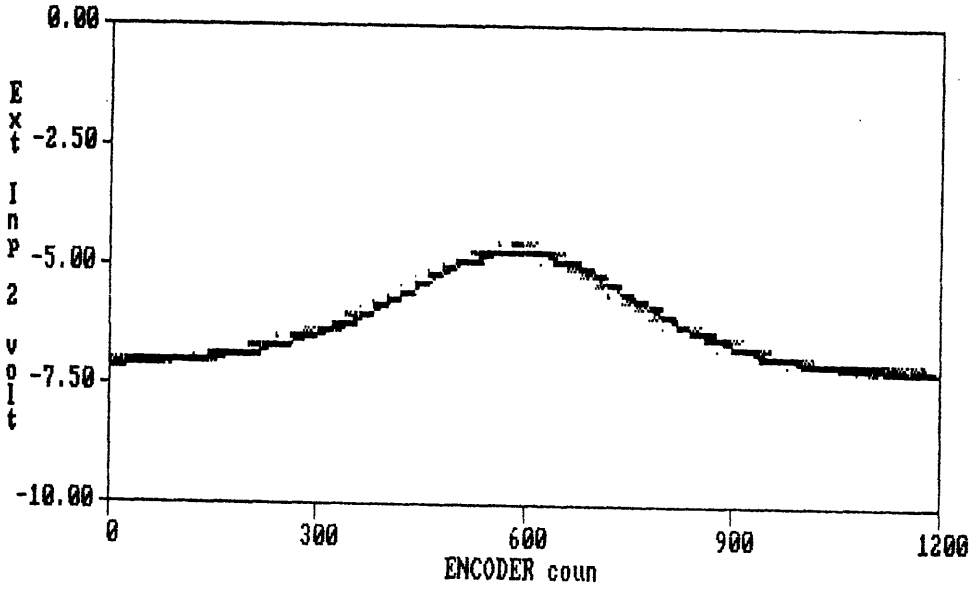

Figure 4.5 Pressure Data of Driven Compressor for a full cycle

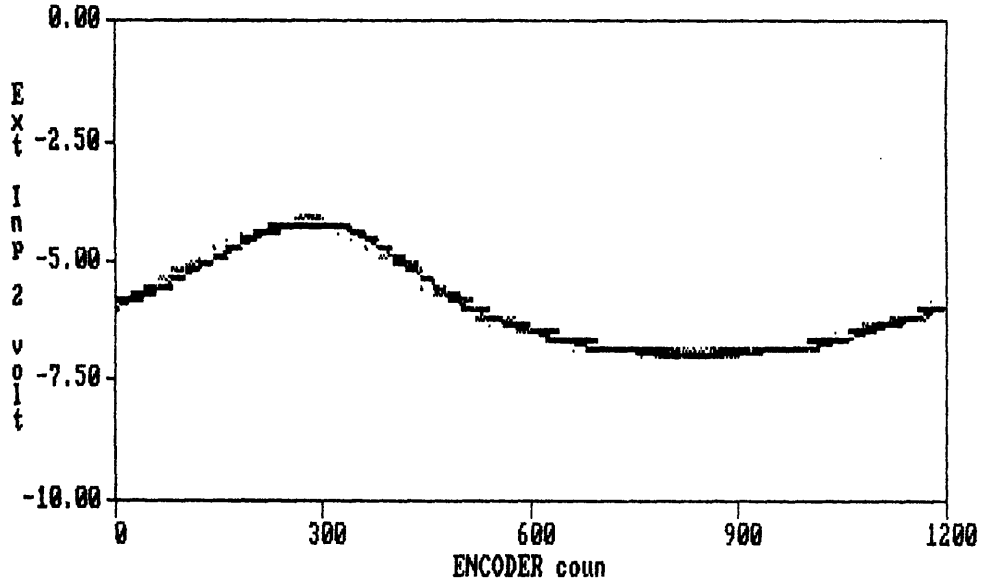

Figure 4.6 Pressure Data of Undriven Compressor for a full cycle

4.7 Other Possibilities

4.7.1 Impaction Effect

Impaction is a phenomenon in which an aerosol jet, issuing from a nozzle, impinges on a plate, and the particles are deposited on it because of their inertia. Since the energy of adhesion of spherical particles to a plane surface is roughly proportional to their diameter and their kinetic energy is proportional to the third power of the diameter and to the square of the velocity, the "critical" particle velocity, above which the particles rebound from impact with the plate, is inversely proportional to their size. From some published data in *Fundamentals of Aerosol Science,* (24, pp. 29-31), the critical velocity is

around a few tens of meters per second for solid particles of size of the order 1μm. In view of our case, the radial flow speed, which causes the seeding particles to collide to the wall is well below the "critical" particle velocity. The deposition efficiency should never come close to 35% which is the maximum, according to the book data. Thus, it cannot provide a sufficient mechanism to account for the phenomenon. Moreover, continuous feeding of seeding particles has been tried but it did not reduce the disappearance appreciably.

4.7.2 Precipitation of Aerosols

Fuchs (6), between 1956 and 1960 published numerous work on the mechanics of aerosols. A part of his work concerns the settling of particles from an aerosol in laminar flow along a horizontal tube of such a small cross-section that vertical convection currents in it are either absent or at least have a velocity that is small compared with the settling rate of the particles. This is relevant to our case as the inner diameter of the test section (1.75 inches) is small enough to neglect vertical convection effect. For a circular tube with viscous flow, the velocity distribution is given by the formula

(4.1) $$U = 2 \cdot \overline{U} \cdot \left(1 - \frac{r^2}{R^2}\right)$$

where,
- r = distance from the axis of the tube
- R = inner radius of the tube
- $\overline{U}$ = average value of the parabolic flow profile.

Then the precipitation efficiency, ɜ in a circular tube is

(4.2) $$ɜ = \frac{2}{\pi} \cdot \left(2\mu\sqrt{1-\mu^{2/3}} + \sin^{-1}\left(\mu^{1/3}\right) - \mu^{1/3}\sqrt{1-\mu^{2/3}}\right)$$

where, $$\mu = \frac{3V_s L}{8R\overline{U}}$$

For a frequency of 1 Hz, R=0.0445m, L=3m, $\overline{U} \cong 18$m/s, and $V_s \cong 0.014$cm/s, μ is found to be 0.0004. Substituting the value in (4.2) gives the precipitation efficiency of less than 0.1%. Almost all of the seeding particles stay in the flow. Even if we take convective diffusion into consideration, calculations show that settling of particles of size between 0.5 and 2 μm takes hours before significant disappearance of particles is observed.

The vertical distribution of dust in horizontal turbulent flow was investigated by Dawes and Slack (6) who blew the dust particles through a pipe. They then measured the concentrations within the pipe at different levels above the bottom of the tube. For particles of size < 8μm, they found the concentration was practically constant throughout the whole cross-section. Not much is found on the wall.

In view of the above, precipitation of seeding particles under the action of gravity and convection in either laminar or turbulent flow does not provide us an explanation.

4.7.3 Thermophoresis

Thermophoresis is particle transport in a temperature gradient. The molecules on the warmer side will move faster, striking the particles more often and also causing greater momentum exchange each time a particle collision occurs. The net force pushes the particles from the warmer area and result in precipitation of the particle on a cold surface.

This may cause the area close to the a hot surface to be free of particles and, under certain conditions, appears as a dark space.

For a particle in the Free Molecule Regime, characterized by $2\lambda/d_p >> 1$ (λ and d_p are mean free path of gas molecules and particles diameter), the thermophoretic velocity u_T and thermal force F_T may be correlated in terms of the thermal dimensionless group Th

(4.3) $$Th = -\frac{u_T \cdot T}{\nu_f \cdot \frac{dT}{dx}}$$

(4.4) $$F_T = \frac{3\pi\mu_f{}^2 d_p}{C\rho_f T} \cdot \left(-Th \cdot \frac{dT}{dx}\right)$$

where C is the Cunningham factor, a correction factor required since the gas no longer behaves as a continuum and is estimated from an equation due to Davies,

(4.5) $$C = 1 + \frac{2\lambda}{d_p}\left[1.257 + 0.400e^{\left(-1.10\frac{d_p}{2\lambda}\right)}\right].$$

dT/dx is the temperature gradient in the direction of flow. Experiments show that the value of Th falls in the neighborhood of 0.5.

Relative importance of thermophoresis may be obtained by estimating u_T in the case of a particle of size 0.1μm in diameter in air of temperature of 80°C and P=1.5 atm. From (4.3), u_T is about (5.01×10^{-4} dT/dx) cm/sec where dT/dx is in °C/cm. It is evident that unless the temperature gradient is very high, say of the order of 1000°C/cm or more, the thermal velocity will not be large enough to be significant. In most situations where

the temperature gradient is much less than 1000°C/cm, F_T is not important in comparison with other forces acting.

4.7.4 Diffusiophoresis

If a gas is a mixture of two kinds of molecules A and B such that there is a difference in concentration between two points, the process of gaseous diffusion will take place according to Fick's Law. If the molecules of B are heavier than A, then small particles ($2\lambda/d_p >> 1$) suspended in the gas will be subjected to bombardment by a greater proportion of B on one side than the other. The particles will take on a net motion in the same direction as the diffusion of B. This process is called diffusiophoresis.

The effect is most significant in the case where the gas (A) is saturated with water vapor (B) surrounded by water droplets as small particles collectors, or known as condensation and evaporation effect. The particle takes on a velocity,

(4.6)
$$u_p = -\frac{\sqrt{m_B}}{n_A\sqrt{m_A} + n_B\sqrt{m_B}} \frac{D_{AB}}{n_A} \frac{\partial n_B}{\partial x}$$

where, m_A or m_B = mass of gas molecule or water vapor,
n_A or n_B = number of gas molecules or water vapor per cm^3,
D = diffusion coefficient
x is positive away from the droplet surface.

Condensation of vapor on the liquid would contribute to capture ($\partial n_B/\partial x > 0$), evaporation of liquid would oppose capture ($\partial n_B/\partial x < 0$). It might first appear not to be too relevant to our case here. Nevertheless, it gives us an upper limit of how important the effect is. For the gas at 65 °C saturated with water vapor and wall of the test section is covered with

water droplets of temperature about 50 °C, the calculation on small particle capture efficiency for particles of size of 1μm by Prem and Pilat is less than a few percent. The smaller the difference, the lower the capture efficiency would be. In the case of the gas temperature being lower than the droplet temperature, the small particles were driven away from the evaporating surface, and the capture efficiency was close to zero.

Again, even though the effect is stronger than that of thermophoresis, it is still far from enough to establish itself as a significant account to what we observed.

4.8 Conclusion of the Investigation

When running the experiments in reverse phase angles (i.e. undriven compressor leads driven compressor) and by constant cleaning of the test section, collection of data points throughout the whole cycle was relatively more successful. This is still not too successful in absolute term.

Chapter 5

Analysis and Experimental Results

There are many mechanical, electrical or thermal systems behaving in much similar a manner to one another. For example, a damped harmonic oscillator is the direct mechanical analog of RLC circuit in an electrical system. Since both systems share precisely the same mathematical form, analysis and experiments on one system can be inferred to those of the other. In this example, the lump of mass takes the role of an inductor in an electrical system, the damping "dash pot" is the resistance and the spring plays the role of the capacitor.

5.1 Complex Nusselt Number Model

There also exists a very similar analogy between thermal and electrical systems. In order to develop a means of correlating heat flux to determine the complex-valued Nusselt number and phase shift between heat flux and ΔT, we might be able to gain some insights from an a.c. circuit. In an a.c. circuit, voltage and current (V and I) are in general out of phase. A complex quantity called phasor was introduced to represent them. And they are held together by another complex quantity, Z impedance ($V = Z \cdot I$). Returning to our case, heat flux takes the role of current, while temperature difference ($\Delta T = T_{CL}-T_W$) plays the role of voltage. The heat transfer coefficient is the reciprocal of impedance or the admittance. Since impedance and admittance is frequency dependent, we can infer that the heat transfer coefficient will not only be complex-valued, but will also assume different

values for different harmonics of the flow. The complex form for Newton's law of convection is:

(5.1) $$q_c = \frac{k}{D_h} \cdot Nu_c \cdot \Delta T_c$$

Rearranging gives:

(5.2) $$Nu_c = \frac{D_h}{k} \cdot \frac{q_c}{\Delta T_c}$$

The complex heat flux and the complex temperature difference between the bulk gas temperature and the wall temperature (real, assumed to be uniform and constant) are expressed in the following forms.

(5.3) $$q_c = \sum_{n=0}^{N} q_n \cdot e^{i(2\pi n\omega t - \phi_{qn})}$$

($q_c > 0$ *denotes heat transfer to the wall)*

(5.4) $$\Delta T_c = T_{CL_c} - T_W = \sum_{n=0}^{N} \Delta T_n \cdot e^{i(2\pi n\omega t - \phi_{Tn})}$$

where for each harmonic:

(5.5) $$h_{C_n} = \frac{q_{C_n}}{\Delta T_{C_n}} = \frac{q_n \cdot e^{i(2\pi n\omega t - \phi_{qn})}}{\Delta T_n \cdot e^{i(2\pi n\omega t - \phi_{Tn})}} = \frac{q_n}{\Delta T_n} e^{-i(\phi_{qn} - \phi_{Tn})}$$

q_n, ϕ_{qn}, ΔT_n, and ϕ_{Tn} are obtained by harmonic decomposition of our measurements. We can then solve for each harmonic of the complex heat transfer coefficient, h_{C_n}.

(5.6) $$h_{C_n} = \frac{q_n}{\Delta T_n} \cdot \cos\left(\phi_{q_n} - \phi_{T_n}\right) + i\frac{q_n}{\Delta T_n} \cdot \sin\left(\phi_{q_n} - \phi_{T_n}\right)$$

Each component of complex Nusselt Number can be obtained from the relationship:

(5.7) $$Nu_{C_n} = \frac{D_h}{k} \cdot h_{C_n}$$

Finally, substituting (5.6) into (5.7) gives

(5.8)
$$Nu_{C_n} = \frac{D_h}{k} \cdot \left[\frac{q_n}{\Delta T_n} \cdot \cos\left(\phi_{q_n} - \phi_{T_n}\right) + i \frac{q_n}{\Delta T_n} \cdot \sin\left(\phi_{q_n} - \phi_{T_n}\right) \right]$$

$$= Nu_C(n) \cdot e^{i(\Delta\phi_n)}$$

where, $\left|Nu_c(n)\right| = \frac{D_h}{k} \cdot \frac{q_n}{\Delta T_n}$ and, $\Delta\phi_n = \phi_{q_n} - \phi_{T_n}$

$\Delta\phi_n$ can be positive as well as negative. A positive $\Delta\phi_n$ simply indicates that the phase of heat flux leads that of temperature difference and a negative value means the opposite. The above analysis and equations were first made and derived by Smith and Yagyu (1991). The magnitude of each harmonic and its associated phase angle can then be determined by running the programs "SMOOTHY6.FOR" and "NUC3.FOR". The first program performs a discrete Fourier Transform on the data and breaks it up into its harmonics, whereas the second program takes the decomposed data and calculates the Complex Nusselt Numbers and the corresponding phase shifts for the first five harmonics.

5.2 Experimental Procedure

Before starting to collect the baseline data, the computer, the LDV system, and the amplifiers for the instrumentation were turned on for a thirty minute warm-up period. This warm-up period was necessary to give time for the amplifiers to settle down and the laser to attain its maximum power.

Each instrument was checked for proper calibration after the warm-up period. The resistance temperature device (RTD) measuring the wall temperature was first calibrated against an alcohol thermometer. From the RTD calibration equation RTD voltage was solved. The potentiometer associated with the amplifier for the RTD was adjusted so that the output voltage (measured with a multimeter) was the same as the solved voltage.

(5.9) $$V_{RTD} = \frac{9/5 \cdot T_{Room}(°C) + 32}{131333}$$

The Kulite high pressure transducer (0-500 psia or 0-3400 kPa) was zeroed to read zero gage pressure at ambient conditions. The output voltage from the pressure transducer's amplifier was converted to psi with the following polynomial calibrated from dead weight pressure meter:

(5.10) $$P_{gage} = (2.595278)V^2 + (60.612839)V + 335.12574$$

where V is the output voltage. Due to the -9 volts offset given by the amplifier's 200 gain, the potentiometer was adjusted to read -9 volts on the multimeter. Output voltages were then converted to absolute pressures [kPa] by the following equation.

(5.11) $$P = \left[P_{gage} + \frac{P_{baro}(14.696 psia)}{29.92 Hg/atm} \right] \cdot \left(\frac{6.895 kPa}{1 psia} \right)$$

The ambient pressure reading P_{baro} was read off from an analog barometer above the power switch.

The RdF heat flux sensor was set to 0.0 volts. The amplifier gain setting was recorded on the data sheet. Since the heat flux readings varied greatly between runs, the amplifier was set at 10,000 for adequate resolution. As a result of such a high

amplifications, the sensor could collect 60 Hz background noise within the laboratory. Thus, it had to be grounded to minimize the noise.

The Beckman Type E traversing thermocouple was calibrated with an alcohol thermometer. The corresponding voltage was found from the following equation through backsolving.

$$T_R = \left(-5.767x10^{-5}\right)V^4 + \left(5.4809x10^{-3}\right)V^3 + (-0.2210)V^2 + (17.0225)V \tag{5.11}$$

V is again the output voltage of the instrument measured after amplification by a multimeter. For all baseline measurements, the thermocouple was positioned at the center of the cross-section of the test section. And the centerline temperature could be safely approximated as the mixed mean temperature as a consequence of the turbulent flow.

We then come to the LDV system. The beams intensity were checked with an optical power meter. The power meter, with the attenuator button on, should be set to the wavelength of the beams (514 nm). The intensity could be balanced by turning the carrier knob. Their intensity must be within 1 mW of each other in order to function properly. Furthermore, each beam needs to have a minimum of 10 mW in intensity. If these requirements are not met, the fiber optic couplers have to be adjusted to the desired value. Lastly, each beam and its reflected beam should be positioned so that they hit the top apex of the glass window and must lie in a vertical plane.

We then move on to set the phase angle, ψ, between the driven and the undriven wheels of the compressors. The bolts on the shrink disks at the driven compressor side

can be loosened to de-couple the two wheels. The undriven wheel was turned to bottom dead center. The encoder installed on the driven wheel was used to register its position. On the computer screen, the ALT-F2 menu of the DSA software was used to monitor the position. Each increment in encoder count amounts to 0.3° of crank angle. Zero Encoder count corresponds to bottom dead center of the driven compressor; a count of 300 sets the phase angle to be 90° and so on. The desired phase angle can be obtained by rotating the wheel and monitoring the reading on the screen. Finally, the two wheels were coupled again by tightening the bolts on the shrink disc.

Lastly, the d.c. motor, driving the compressors was turned on. Initial runs were performed to check for the correct pressure. The ratio can be corrected to approximately 2.0 by adjusting the two dead volumes on each compressors. Whenever an adjustment on one variable dead volume is made, an equal adjustment on the other one must be made, too. It is important that the dead volumes be the same on both compressors.

Then, the system was ready to take data. During data acquisition, the oscilloscope had to be on. One trace on the oscilloscope showed the signal from OUT BNC of the Doppler Signal Analyzer and the other trace was from the ANALOG BURST DETECTORS. Fuzzy bursts could be seen from the first output. The threshold in F3 page could be monitored to filter out noise; every time a burst reached over that level, a 5-Volt "up" signal could be observed from the Analog Burst Detectors on the oscilloscope. This line also means that the DSA could register and process the "up" signal. The data

was collected in two separate runs due to insufficient channels on the A/D converter. The first run collected both the pressure and the heat flux; the second one collected the centerline and the wall temperatures. The frequency could be varied by simply varying the voltage of the auto transformer supplying power to drive motor. The belt setting could be adjusted to either high or low speed belt settings. The low belt setting allowed the motor to drive the system from 0.08 to 0.98 Hz, whereas the high belt setting let the frequency take a value between 1.5 and 8.25 Hz.

Between each data collection at different frequencies, the apparatus had to be allowed at least five minutes to let the system settle to steady state condition. Once all the data was collected over the entire range of the system, the phase angle between the compressors was changed to the next value for another data collection.

5.3 Experimental Results

As a result of the difficulties in the seeding of the flow, it was impossible to collect sufficient good LDV data to generate useful fluid velocity distribution. However, other baseline experimental data (Appendix B) were collected at compressors phase angle settings of Ψ=0°, 45°, 90°, 135°. From full data set graphs (Fig 5.1-5.8), there is a clear indication that phase shift exists between heat flux and the temperature difference at all four phase angles. The phase shift is obvious at two separated frequencies. At low frequencies or oscillating Peclet number Pe_ω (Fig 5.1, 5.3, 5.5, 5.7), the temperature difference leads heat flux. This phase shift between temperature difference and heat flux

is reduced and reach zero difference for increasing Pe_ω. Eventually, heat flux will lead temperature as Pe_ω is further increased (Fig 5.2, 5.4, 5.6, 5.8). This finding is consistent to that of Grassmyer in 1994.

Results were achieved for each harmonic by decomposing the variables into their harmonics. The graph of magnitude of the first harmonic complex Nusselt number, or $|Nu_{c1}|$ at each phase angle (Fig 5.9), shows that the amplitude of the first harmonic generally increases with Pe_ω. Moreover, the curve is shifted up, by advancing the compressors phase angle. These results are consistent and serve as an extension to Grassmyer's findings. However, there is an aspect which does not quite agree with his finding; the values, $|Nu_{c1}|$ never rise as high as the 700 level. They stay between 0 and 350. As for magnitude of the second harmonic complex Nu, $|Nu_{c2}|$, similar trends were discovered. Again, it is consistent with what the previous experimenter discovered, but the values are twice as large as before.

As we come to the first harmonic phase shift (Fig 5.11), first harmonic temperature difference leads that of heat flux. This phase lead is then reduced to zero and becomes negative. The magnitudes correlated quite well with Peclet number for all of the compressors phase angle in general, except at zero degree, with a small amount of noise at the higher frequency range. The scatter at zero degrees may result from the relatively low heat flux and temperature difference for the whole experiment range. Under that condition, noise, very likely picked up from the amplifiers with high gain values, may be

comparable to the values of heat flux and temperature difference. This noise can add unexpected distortion to phase shift value. Phase shift is more susceptible to noise than the magnitude of the Nusselt number. This can be understood in a sense that the noise amplitude is rather small and averaged out to zero. However, phase can be changed in an unknown fashion by noise, composing of high frequencies, at different phases. As a result, higher harmonics are more likely to be affected. As for the second harmonic phase shift (Fig 5.12), it is even more prone to noise problem. There is scatter in the plots which is more prominent at high frequency. Overall, no clear indication of trend was observed. However, at frequencies where noise effect is not as strong, the trends are consistent with those found by Grassmyer (8); the phase shift between heat flux and temperature difference decreases with Peclet number.

5.4 Complex Nusselt Number Correlations

A least square method was used to find the best fit to the experimental data. For a system of equations,

(5.12) $$\mathbf{Ax=B}$$

since **x** may not always be a unique solution, a least error solution could then be found by multiplying both side by $\mathbf{A^T}$ and solving the resulting system of equation.

(5.13) $$\mathbf{A^TAx=A^TB}$$

Both linear and quadratic fits were found.

Ψ=0°:

$|Nu_1|=1.7092Pe_\omega+34.2970$; $|Nu_1|=-0.0003Pe_\omega^2+1.7540Pe_\omega+32.8079$
$|Nu_2|=5.0872Pe_\omega-37.7158$; $|Nu_2|=0.0153Pe_\omega^2+2.4766Pe_\omega+49.0491$

$\Psi=45°$:

$|Nu_1|=1.5730Pe_\omega+67.4800$; $|Nu_1|=0.0006Pe_\omega^2+1.4705Pe_\omega+70.8085$
$|Nu_2|=4.5764Pe_\omega+55.8685$; $|Nu_2|=0.0584Pe_\omega^2-4.7917Pe_\omega+359.6373$

$\Psi=90°$:

$|Nu_1|=2.0409Pe_\omega+82.9371$; $|Nu_1|=-0.0156Pe_\omega^2+4.7323Pe_\omega-11.7598$
$|Nu_2|=7.1143Pe_\omega-97.6706$; $|Nu_2|=-0.0109Pe_\omega^2+9.0022Pe_\omega-164.0972$

$\Psi=135°$:

$|Nu_1|=2.2635Pe_\omega+129.1648$; $|Nu_1|=-0.0113Pe_\omega^2+4.1709Pe_\omega+63.5478$
$|Nu_2|=6.0737Pe_\omega-19.5431$; $|Nu_2|=0.0358Pe_\omega^2+0.0028Pe_\omega+189.3086$

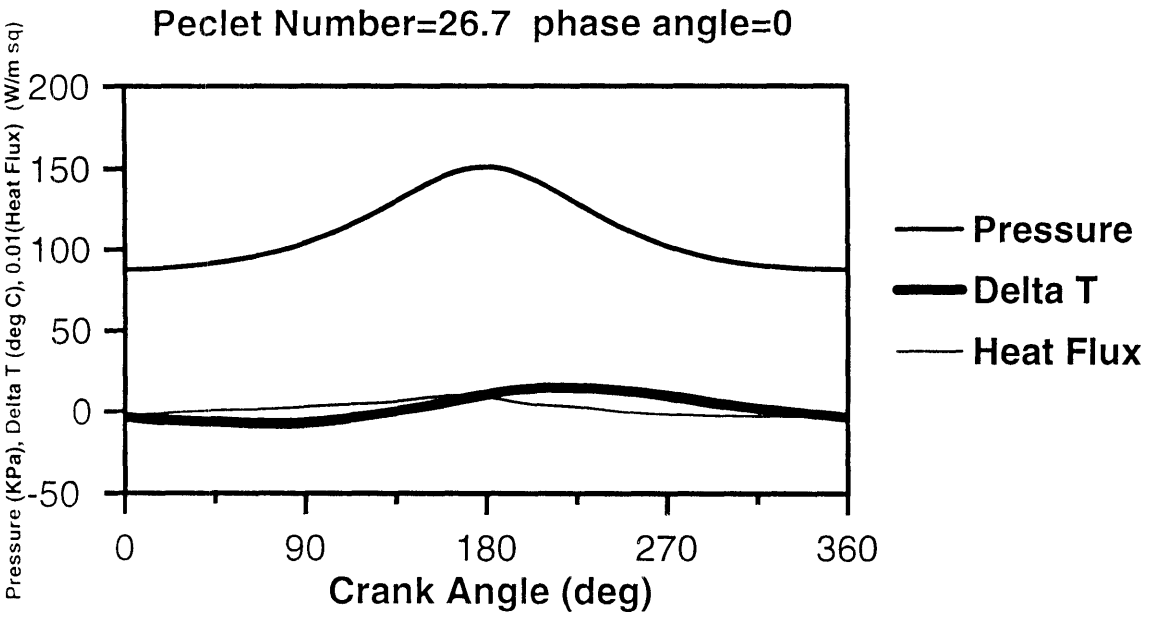

Figure 5.1 Full Data set at Pe_{ω}=26.7, Ψ=0°

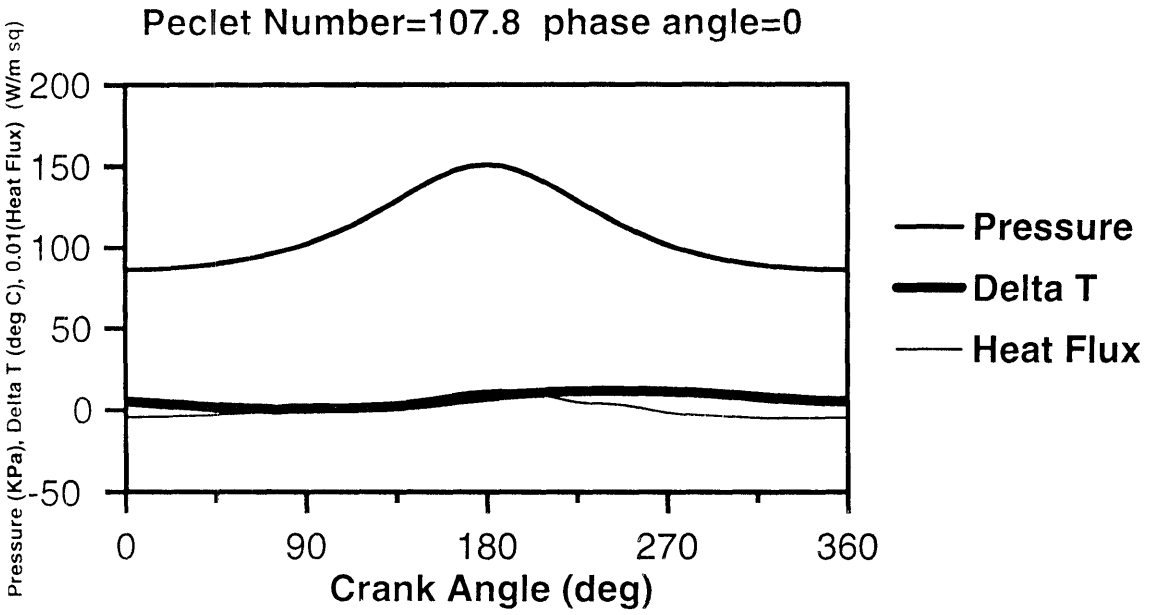

Figure 5.2 Full Data set at Pe_{ω}=107.8, Ψ=0°

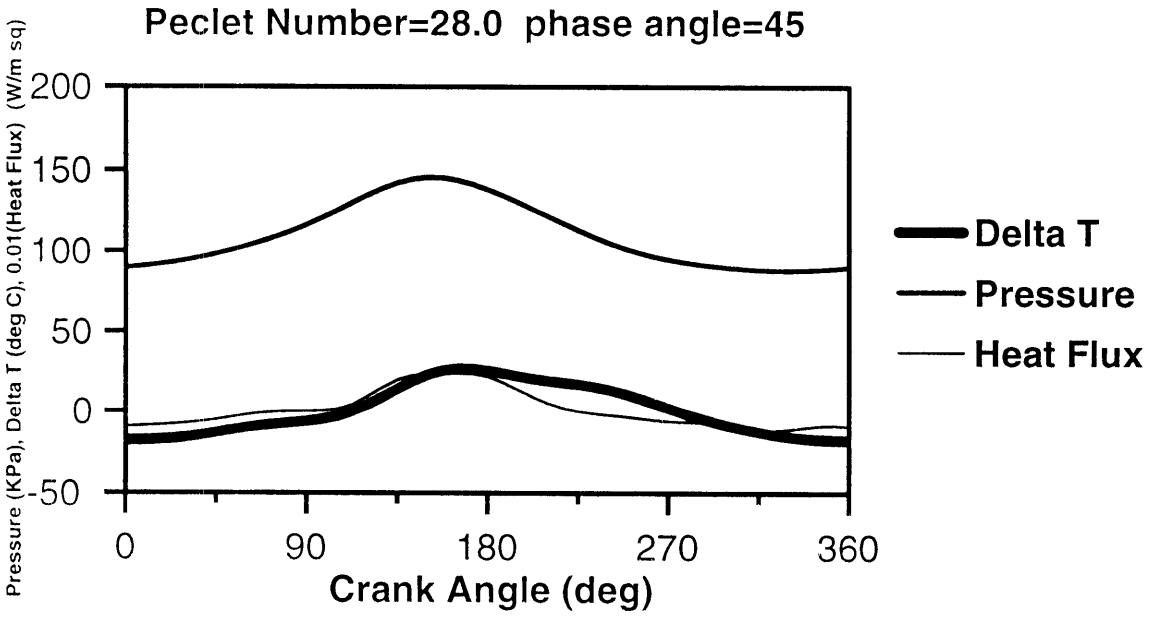

Figure 5.3 Full Data set at Pe_{ω}=28.0, Ψ=45°

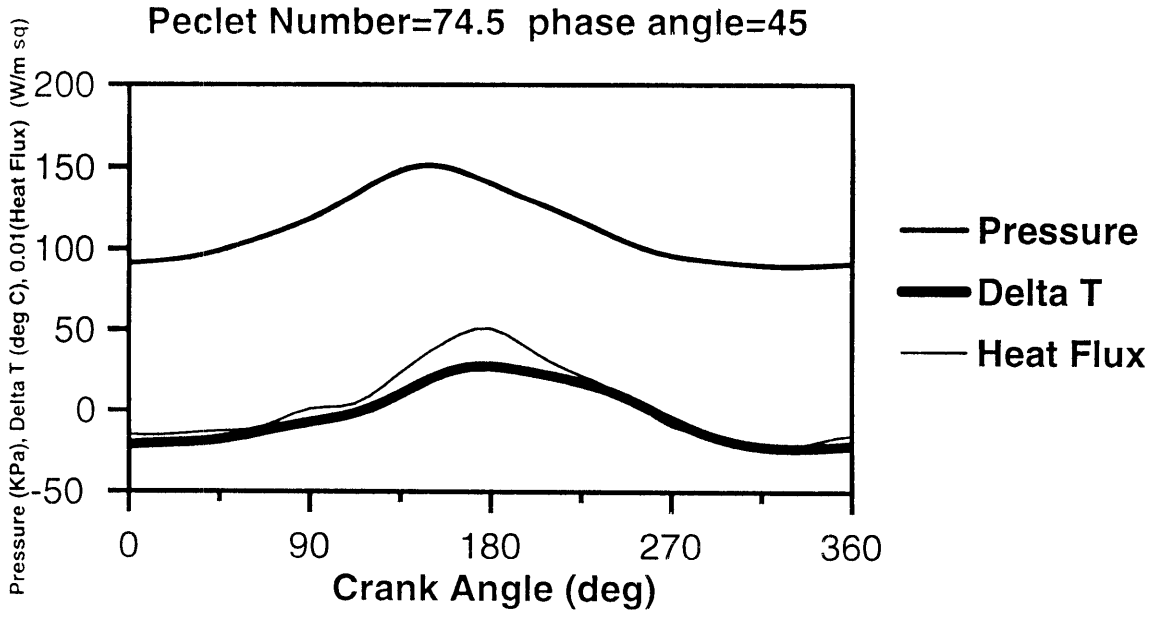

Figure 5.4 Full Data set at Pe_{ω}=74.5, Ψ=45°

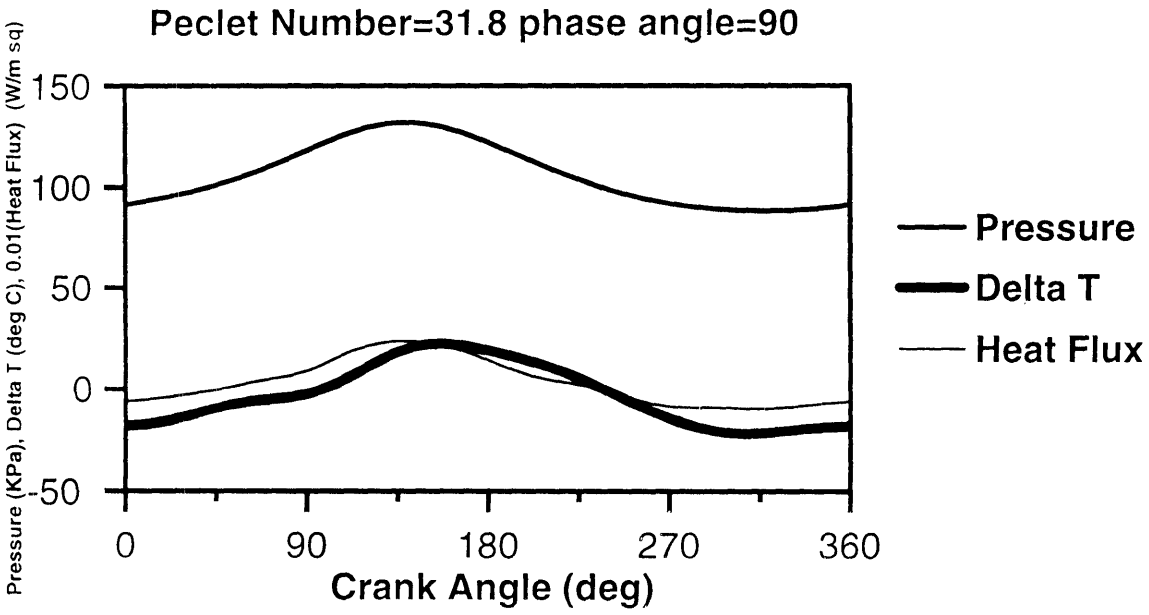

Figure 5.5 Full Data set at Pe_{ω}=31.8, Ψ=90°

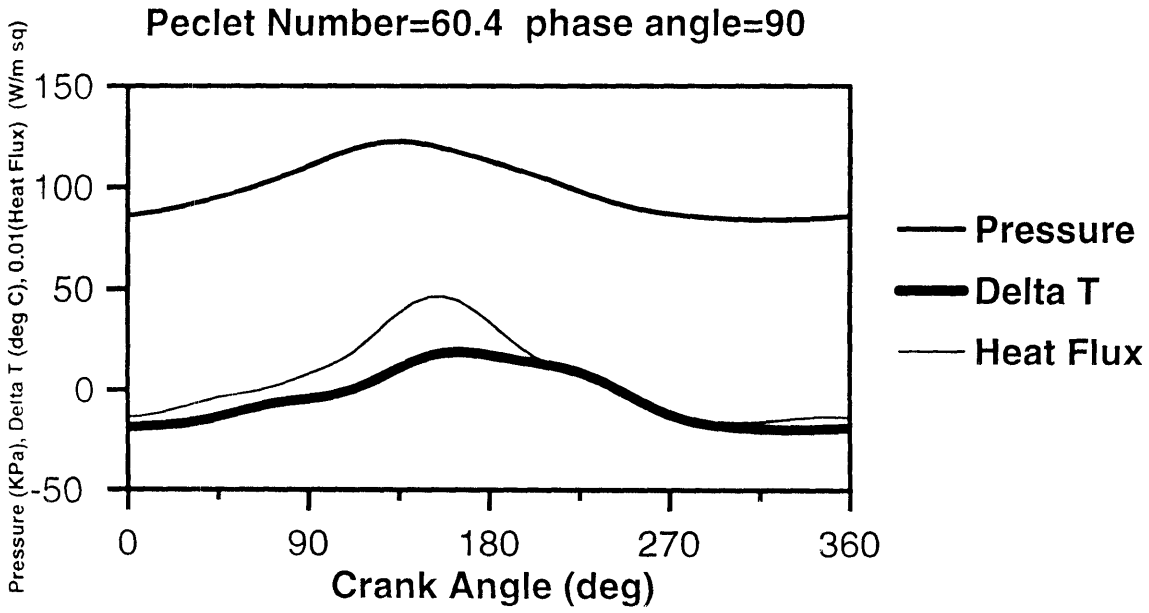

Figure 5.6 Full Data set at Pe_{ω}=60.4, Ψ=90°

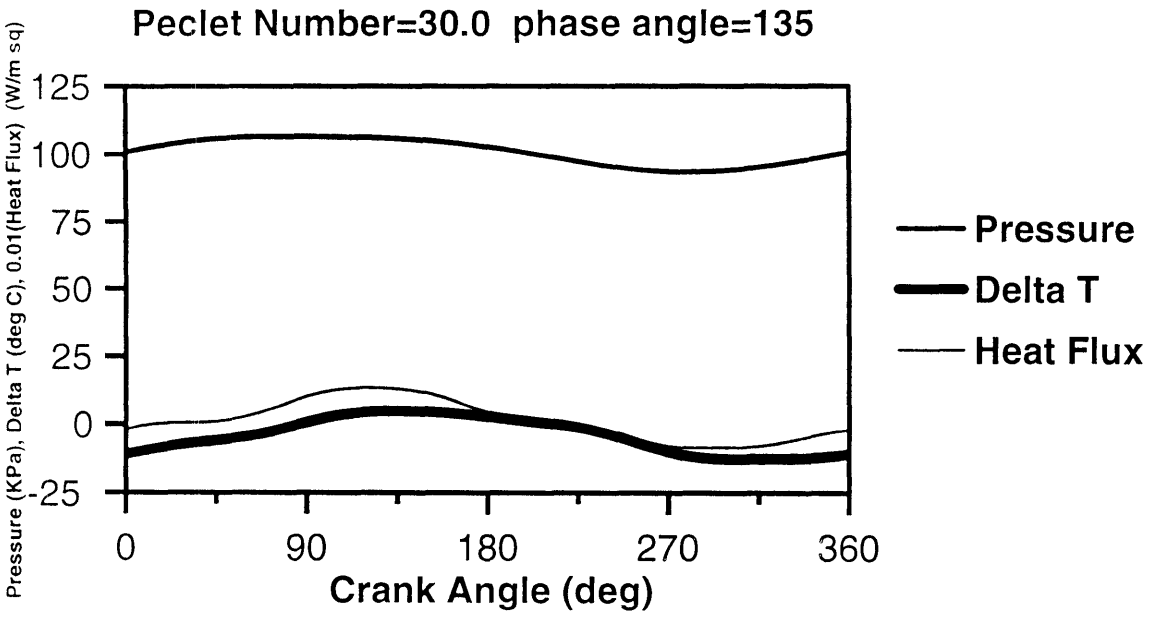

Figure 5.7 Full Data set at Pe_{ω}=30.0, Ψ=135°

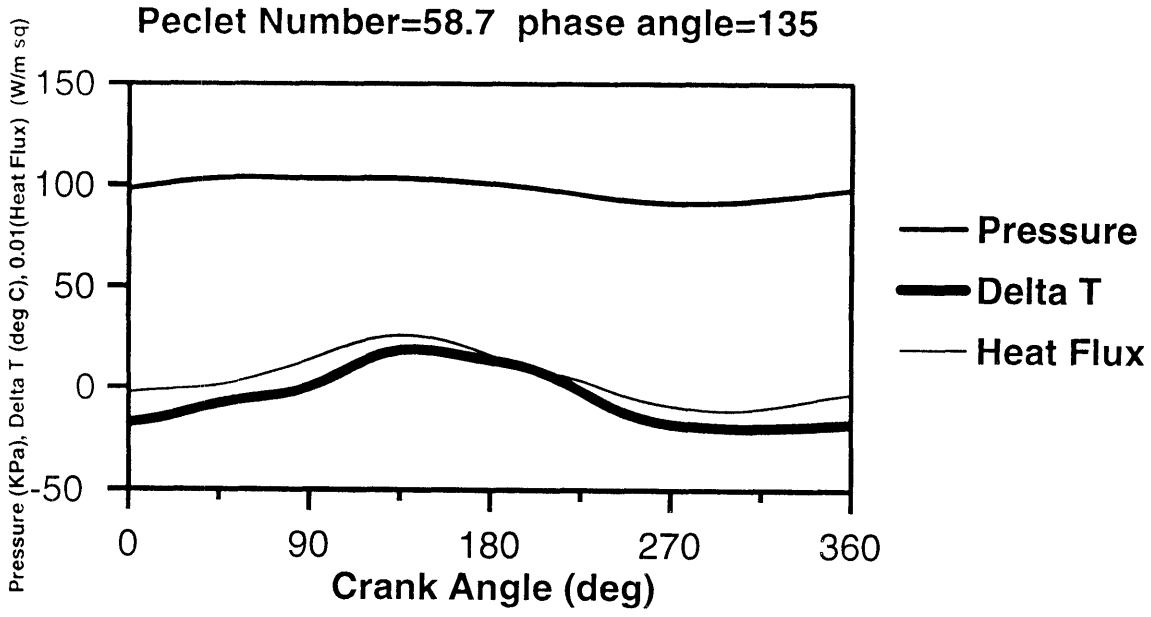

Figure 5.8 Full Data set at Pe_{ω}=58.7, Ψ=135°

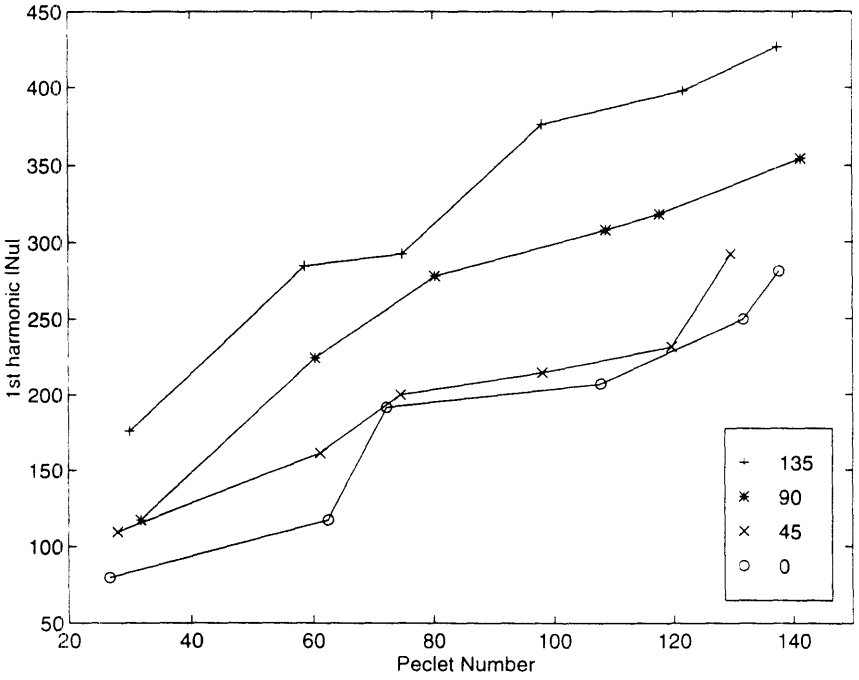

Figure 5.9 1st harmonic $|Nu_C|$ as a function of Pe_ω

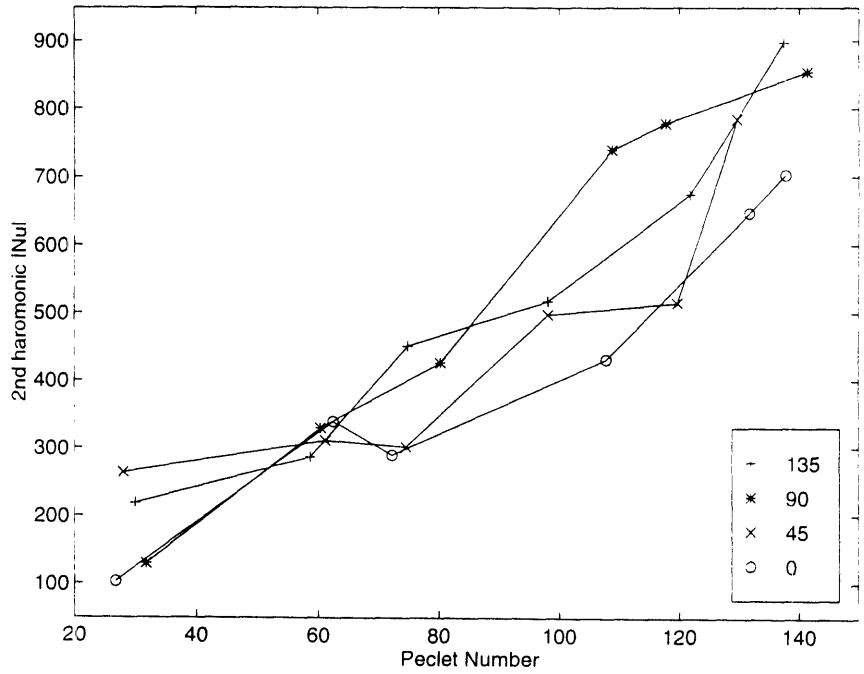

Figure 5.10 2nd harmonic $|Nu_C|$ as a function of Pe_ω

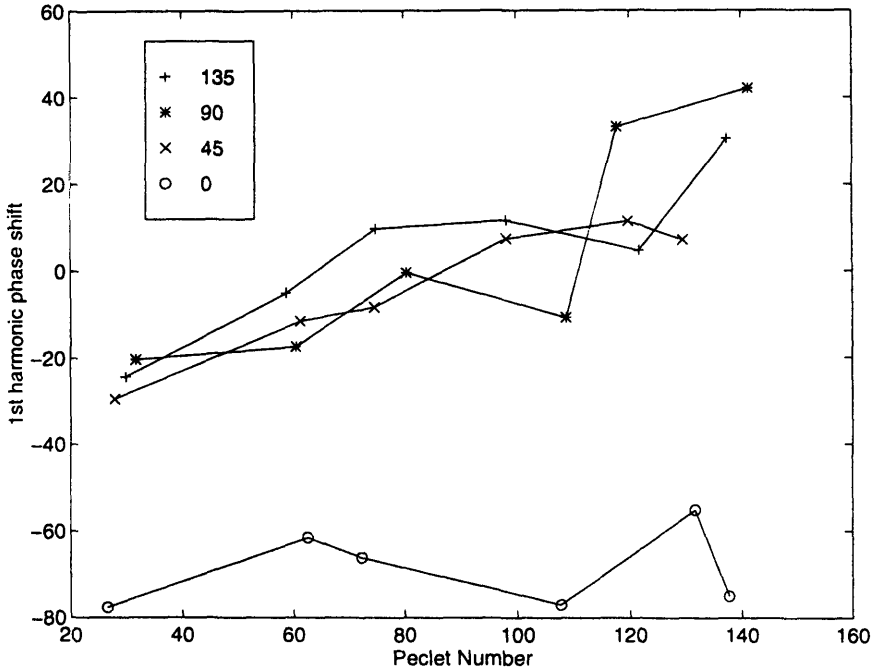

Figure 5.11 1st harmonic Phase Shift as a function of Pe_ω

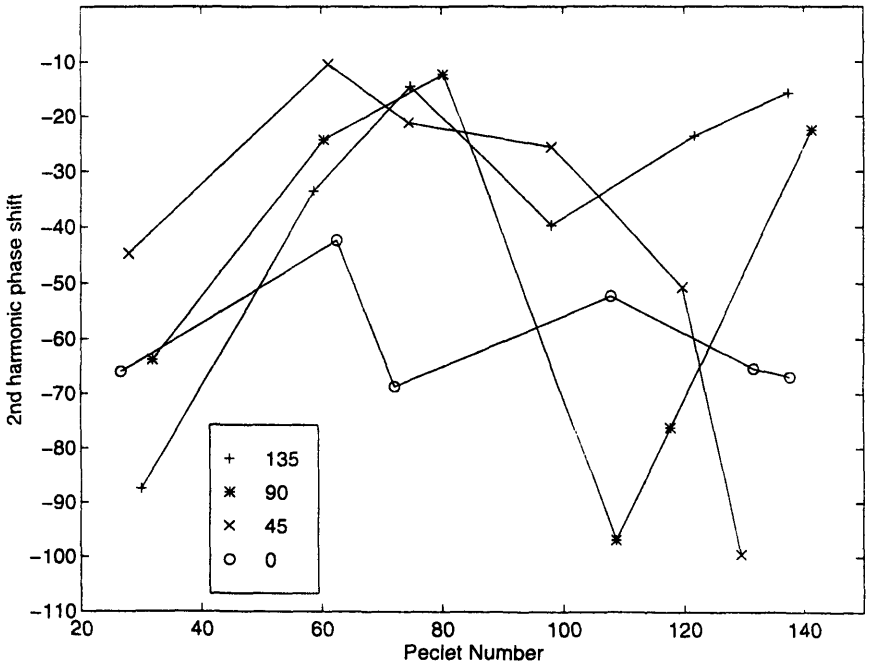

Figure 5.12 2nd harmonic Phase Shift as a function of Pe_ω

Chapter 6

Conclusion

6.1 Summary of the Study

These experiments of collecting baseline data have confirmed the existence of phase shift between heat flux and temperature difference under the oscillatory conditions which show that Newton's law of convection has to modified. The model of complex Nusselt number serves as a means to describe and predict heat transfer as a result of this phenomenon. The most significant findings are as follows.

1) The experiments clearly display the phase shift phenomenon between heat flux and ΔT for a gas under conditions of oscillating pressure and flow. The phase shift is a function of Pe_ω and compressors phase angle, Ψ.
2) First and second harmonic complex Nusselt numbers indicate a somewhat linear relationship with Pe_ω. Also, they have a linear relationship with compressors phase angle, Ψ. First and second harmonic phase shift show a similar linear trend with Pe_ω and with compressors phase angle, Ψ.
3) Consistent results were obtained with the previous findings. The results were extended to compressors phase angles of 90° and 135°. Disagreement with Dean's result was repeated and confirmed.

4) The use of Talcum powder is not an effective choice as seeding particles for LDV system under oscillating conditions. Successful data acquisition is rare and, frequent cleaning of test section is needed to ensure this rare rate of success.

5) Noise in all instrumentation is still a major problem and a threat to the ultimate reliability of the data acquired.

6.2 Recommendations for Future Work

Even though the whole apparatus has gone through several phases of modifications. There is still room for improvement.

- A study should be carried out as to why data points could be taken for most parts of the cycle at reverse phase angles but not vice versa. A much more careful investigation of the compressors would be helpful.
- Noise problem still exists and should be further minimized as much as possible. It remains a threat to the accuracy of the correlation obtained.
- If funding allows, a pair of improved version optical couplers should be purchased to facilitate the alignment of the laser. The existing ones are unstable and loose after years of service.

Appendix A

A.1 Data Smoothing and Fourier Decomposition Program, "SMOOTHY6"

```
C*********************************************************
C                                                        *
C  This program takes the raw data and breaks it up into *
C  it's harmonics. This output of this program is used   *
C  by NUC1 which determines the complex Nusselt Number.  *
C           By  William A. Grassmyer                     *
C                                                        *
C*********************************************************

    CHARACTER*32 INPUT,DI
    CHARACTER*12 CH,DV,CR1,CR2
    CHARACTER AUTO*3,RUN*2,OUT*7,VOLT*3,FL*4,PH*3,ZY*1

    DIMENSION V(4000),T(4000),EX1(4000),EX2(4000),KEN(4000),CH(2),
   *VN(4000),TN(4000),EX1N(4000),EX2N(4000),KENN(4000),EN(4000),
   *XSIN(200),XCOS(200),A(20),B(20),A1(20),B1(20),A2(20),B2(20)
   *,IC(50),XX(20),V1(361),CX1(361),CX2(361),XV(361),XC1(361),
   *XC2(361),VT(361)

    WRITE(*,*)'INPUT BAROMETRIC PRESSURE(IN. HG):'
    READ(*,*) BARO
    WRITE(*,*)

 83 WRITE(*,14)
 14 FORMAT(/,5X,'COMBINE TWO FILES?',/,9X,'1) NO',/,9X,'2) YES',/)
    READ(*,*) LF
    IF(LF.NE.1.AND.LF.NE.2) GOTO 83

    WRITE(*,*)
    WRITE(*,*)'INPUT THE VOLTAGE OF RUN(EX 050):'
    READ(*,'(A3)') VOLT

    WRITE(*,*)
    WRITE(*,*)'INPUT BELT SETTING(EX HIGH OR LOWB)'
    READ(*,'(A4)') FL
    WRITE(*,*)
    OUT=VOLT//FL
    WRITE(*,*) OUT
C    WRITE(*,*)'INPUT NAME OF OUTPUT FILE(EX 0500200):'
C    READ(*,517) OUT
517  FORMAT(A7)

    WRITE(*,*)
    WRITE(*,*) 'PHASE ANGLE (EX. 045):'

    READ(*,'(A3)') PH
    WRITE(*,*) 'PHASE ANGLE (EX 45.):'
    READ(*,'(F6.2)') PHI
```

```
      WRITE(*,*) 'HEAT FLUX AMPLIFICATION:'
      READ(*,*) HFA


      WRITE(*,*) 'OTHER INFO ON DATA (32 CHARACTER MAX):'
      READ(*,511) DI
  511 FORMAT(A32)

      OPEN(UNIT=7,FILE='C:\COEF\'//PH//'\'//OUT//'.COF',
     *STATUS='UNKNOWN')
      OPEN(UNIT=9,FILE='C:\CYCLE\'//PH//'\'//OUT//'.DAT',
     *STATUS='UNKNOWN')



      DO 377 MF=1,LF
  999 WRITE(*,*)'INPUT NUMBER OF TEST DIRECTORY (EX 003)'
      READ(*,'(A3)') AUTO
      IF(AUTO .LE. ' ') GOTO 999
  518 FORMAT(A11)
      WRITE(*,*)

       WRITE(*,*)'INPUT RUN NUMBER OF FILE (EX 07):'
       READ(*,'(A2)') RUN
       WRITE(*,*)

      OPEN(UNIT=3,FILE='C:\DSA4\DSADATA\EXPNAME\TEST'//AUTO//'\'
     *//'RUN'//RUN//'\DSARAW.TXT',STATUS='OLD')
      READ(3,*)

      WRITE(*,*)'C:\RAW\T'//AUTO//'R'//RUN//'.RAW'

      OPEN(UNIT=21,FILE='C:\RAW\T'//AUTO//'R'//RUN//'.RAW',
     *STATUS='UNKNOWN')

   2  FORMAT(/,/,5X,'ENTER THE CORRECT #:',/,10X,'1) PRESSURE',
     */,10X,'2) HEAT FLUX',/,10X,'3) TEMP THERMOCOUPLE',/,10X
     *,'4) TEMP RTD',/,10X,'5) NO CALIBRATION')
      WRITE(*,2)
      WRITE(*,3)
   3  FORMAT(/,5X,'FOR EXT INPUT #2:')
      READ(*,*) KX1
   4  FORMAT(/,5X,'FOR EXT INPUT #3:')
      WRITE(*,4)
      READ(*,*) KX2
  19  FORMAT(5F14.6)

C*************************************************************
C  THE DATA IS READ IN IN LINE 5.                  *
C  NP= NUMBER OF POINTS OF RAW DATA, EX1&EX2= EXTERNAL INPUTS *
C  V= VELOCITY, EN= ENCODER POSITION,T= TIME              *
C*************************************************************
```

```
    NP=1
C349  FORMAT(E15.6E4,2X,E15.6E4,2X,E15.6E4,2X,E15.6E4,2X,E15.6E4)
C 349  FORMAT(F9.6,2X,F11.6,2X,F9.6,2X,F9.6,2X,F9.6)


C  5  READ(3,349,END=8) V(NP),EN(NP),EX1(NP),EX2(NP),T(NP)
   5  READ(3,*,END=8) V(NP),EN(NP),EX1(NP),EX2(NP),T(NP)
C     WRITE(21,19) V(NP),EN(NP),EX1(NP),EX2(NP),T(NP)
     WRITE(*,19) V(NP),EN(NP),EX1(NP),EX2(NP)
C     PAUSE
     NP=NP+1
     GOTO 5

   8  NP=NP-1

     DO 88 I=1,NP
  88  KEN(I)=EN(I)

     NOP=NP

C*****************************************************************
C  SUBROUTINE SMOOTH EXAMINES THE VELOCITY DATA AND REJECTS ANY *
C  EXTRANEOUS VELOCITY READINGS.  THIS WAS DONE BECAUSE THE LDV *
C  SYSTEM SOMETIMES READS RANDOM NOISE AS A DOPPLER BURST     *
C*****************************************************************

     CALL SMOOTH(V,EX1,EX2,T,KEN,NP,VN,TN,EX1N,EX2N,KENN)

C     DO 27 I=1,NP
C  27 WRITE(*,*) KENN(I),VN(I)
C     PTO=NOP-NP
C     WRITE(*,*) PTO,NP
C     PAUSE
C*************************************************************
C  THE NEXT GROUP OF LINES DETERMINES HOW MANY CYCLES OF    *
C  DATA WERE TAKEN.  THIS WAS DONE BY DETERMINING WERE THE  *
C  ENCODER RESETS. IF LESS THAN ONE CYCLE OF DATA WAS TAKEN *
C  THE PROGRAM KICKS OUT AND DISPLAYS AN ERROR MESSAGE.     *
C  THE PERIOD OF ROTATION, PERA, IS ALSO DETERMINED.        *
C*************************************************************
     JT=0
     DO 20 IT=2,NP
     IF (KEN(IT)+10.LT.KEN(IT-1)) THEN
       JT=JT+1
       IC(JT)=IT
     ENDIF
  20  CONTINUE

     IF(JT.GE.2) GOTO 474

     IF(JT.EQ.1) THEN
       DO 59 I=IC(1),NP
```

```
      IF(KEN(2).LE.KEN(I)) THEN
        PERA=T(I)-T(2)
        GOTO 889
      ENDIF
 59  CONTINUE
    ENDIF
    WRITE(*,*) 'ERROR: ONE FULL PERIOD OF DATA WAS NOT TAKEN'
    GOTO 701

474  PS=0
    DO 63 I=2,JT
     I1=IC(JT-1)
     I2=IC(JT)
     PER=T(I2)-T(I1)
 63   PS=PS+PER
     PERA=PS/REAL(JT-1)

 889  CONTINUE

C*************************************************************
C  SUBROUTINE SORT TAKES THE DATA SETS AND SORTS IT BY THE   *
C  ENCODER POSITION.                                         *
C*************************************************************

    WRITE(*,*) 'LEAVE ME ALONE DAMMIT! IM SORTING'
    CALL SORT(V,EX1,EX2,NP,T,KEN)

C*************************************************************
C  INORDER TO PERFORM A FOURIER DECOMPOSITION THE DATA HAD TO *
C  BE ARRANGED AT EQUAL TIME INTERVALS.  SUBROUTINE GROUP    *
C  TAKES THE DATA AND SEPARATES IT INTO 7.5 DEGREE WINDOWS.  *
C  THE AVERAGE VALUE OF EACH WINDOW IS THEN DETERMINED.  IF  *
C  THERE IS NO DATA IN A PARTICULAR WINDOW,  AN AVERAGE VALUE *
C  IS INTERPOLATED FROM THE DATA WINDOWS ON EACH SIDE        *
C*************************************************************

    CALL GROUP(NP,V,EX1,EX2,T,KEN,NW,VN,EX1N,EX2N,TN,KENN)

C*************************************************************
C  SUBROUTINE CONVRT CONVERTS THE DATA FROM VOLTS TO ITS     *
C  ITS RESPECTIVE UNITS.                                     *
C*************************************************************

    CALL CONVRT(KX1,KX2,NW,EX1N,EX2N,CH,BARO,HFA)

C*************************************************************
C  SUBROUTINE FORIER TAKES THE AVERAGED DATA AND DECOMPOSES   *
C  IT INTO IS HARMONICS.  M= THE NUMBER OF HARMONICS          *
C*************************************************************

    M=5
    TIME=1200
    LLX=0
```

```
      FRQ=1./PERA

      CALL FORIER(NW,M,TIME,VN,KENN,A0,A,B,XSIN,XCOS,LLX,FRQ)

      IF (KX1.EQ.2) THEN
       LLX=1
      ENDIF

      CALL FORIER(NW,M,TIME,EX1N,KENN,A01,A1,B1,XSIN,XCOS,LLX,FRQ)
      LLX=0
      IF (KX2.EQ.2) THEN
       LLX=1
      ENDIF

      CALL FORIER(NW,M,TIME,EX2N,KENN,A02,A2,B2,XSIN,XCOS,LLX,FRQ)

C*************************************************************
C  THE VOLUME WAS THEN CALCUALTED FOR EVERY 7.5 DEGREES     *
C*************************************************************

      DO 118 I=1,NW
       POS=REAL(KENN(I))/1200.
       PI=3.1415927
       RAD=2.*PI*POS
       VL=PI*11.**2./8.*(30.+9.*(1.+COS(RAD))-SQRT(
     *  (9.*COS(RAD))**2+819.))
       VR=PI*11.**2./8.*(30.+9.*(1.+COS(RAD-PHI))-SQRT(
     *  (9.*COS(RAD-PHI))**2+819.))
       VTS=371.21+(2.00*16.84)
       VFDV=(2.*726.)*1.6387*10.**(-5)
       VADV=0.
       VTDV=VFDV+VADV
 118   VT(I)=(VL+VR+VTS)*1.6387*10.**(-5)+VTDV



C*************************************************************
C  RESULTS WERE THEN OUTPUTTED TO 2 DIFFERENT FILES.  THE .COF *
C  FILES CONTAIN ALL THE COEFICIANTS FOR THE DECOMPOSED       *
C  HARMONICS AND THE FREQUENCY OF ROTAION OF THE SYSTEM.  THIS *
C  FILE IS USED BY THE PROGRAM NUC1.  THE .DAT FILES CONTAINS  *
C  DATA FOR EACH 7.5 DEGREE WINDOW USING THE HARMONICS.       *
C*************************************************************


C**********************OUTPUT TO .COF FILES*********************

 716  FORMAT(/,/,5X,'DIRECTORY  = AUTO',A1,'\RUN',A2,/)
      WRITE(7,716) AUTO,RUN
      IF(MF.EQ.1) THEN
       WRITE(7,717) VOLT,FL,PH,VTDV,BARO,DI
      ENDIF
```

```
717  FORMAT(5X,'VOLTAGE   = ',A6,/,5X,'FLOW POSN  = ',A6,/,5X,
    *'PHASE ANGLE= ',A6,/,5X,'DEAD VOLUME= ',F7.5,/,5X,
    *'BARO PRESS = ',F7.3,/,5X,'NOTE      = ',A32)



     WRITE(7,555) CH(1),CH(2)
555  FORMAT(/,/,25X,'FOURIER COEFFICIENTS',/,/,2X,'HARMONIC',8X,
    *'VELOCITY',10X,A12,10X,A12,/,/,16X,'A',7X,'B',12X,'A',8X,'B',
    *12X,'A',8X,'B')

     I=0
     WRITE(7,566) I,A0,A01,A02
566  FORMAT(4X,I2,6X,F7.3,13X,F8.3,14X,F8.3)

     DO 700 I=1,M
700  WRITE(7,699) I,A(I),B(I),A1(I),B1(I),A2(I),B2(I)

699  FORMAT(4X,I2,6X,F7.3,2X,F7.3,4X,F8.3,2X,F8.3,4X,F8.3,2X,F8.3)

     WRITE(7,577) PERA
577  FORMAT(/,5X,'PERIOD=',F7.4,' SEC')

C***************OUTPUT TO .DAT FILE*****************************



     DO 12 I=1,NW
     POS=REAL(KENN(I))/1200.
     TIM=POS*PERA
     V1(I)= CURV(POS,A0,A,B,M,XX)
     CX1(I)= CURV(POS,A01,A1,B1,M,XX)
 12  CX2(I)= CURV(POS,A02,A2,B2,M,XX)

     IF(LF.EQ.1) GOTO 323

C**********COMBINING TWO RUNS*****************

     IF(MF.EQ.1) THEN
       CR1=CH(1)
       CR2=CH(2)
       XPER=PERA
      DO 43 I=1,NW
       XV(I)=V1(I)
       XC1(I)=CX1(I)
43     XC2(I)=CX2(I)
    ELSE
     WRITE(9,61) CR1,CR2,CH(1),CH(2)
61    FORMAT(4X,'DEGS',1X,'TIME',5X,'VEL',2X,'VOL',4X,
    *  A9,1X,A9,4X,A9,1X,A9,/)

      PERM=(XPER+PERA)/2.
```

```
      I=0
      DEG=0.
      TIM=0
      VA=(XV(NW)+V1(NW))/2.

      WRITE(9,89) DEG,TIM,VA,VT(NW),XC1(NW),XC2(NW),CX1(NW),CX2(NW)
      DO 47 I=1,NW
       POS=REAL(KENN(I))/1200.
       DEG=POS*360.
       TIM=POS*PERM
       VA=(XV(I)+V1(I))/2.
 47     WRITE(9,89) DEG,TIM,VA,VT(I),XC1(I),XC2(I),CX1(I),CX2(I)
    ENDIF
 89  FORMAT(2X,F5.1,F7.3,F8.3,F8.4,F10.4,F13.1,2F10.4)

    GOTO 377
C**************JUST ONE FILE************************

 323  WRITE(9,921) CH(1),CH(2)
 921  FORMAT(1X,'ENC POS',9X,'TIME',9X,'VELOCITY',7X,A12
    *,3X,A12,/)

    TIM=0
    I=0
    WRITE(9,422) I,TIM,V1(NW),CX1(NW),CX2(NW)
    DO 324 I=1,NW
    POS=REAL(KENN(I))/1200.
    TIM=POS*PERA
 324  WRITE(9,422) KENN(I),TIM,V1(I),CX1(I),CX2(I)

 422  FORMAT(2X,I5,4F15.4)

 377  CONTINUE

 701  WRITE(*,485)
 485  FORMAT(/,/,5X,'WANT TO RUN AGAIN?',/,9X,'1) YES',/,9X,'2) NO',/)
    READ(*,*) NNN
    IF(NNN.EQ.1) GOTO 83

    END


C********************SUBROUTINES START HERE************************

    SUBROUTINE SMOOTH(V,EX1,EX2,T,KEN,NP,VN,TN,EX1N,EX2N,KENN)

    DIMENSION V(NP),T(NP),EX1(NP),EX2(NP),KEN(NP),VN(NP),TN(NP)
   *,EX1N(NP),EX2N(NP),KENN(NP)

    IN=NP/10.
    NC=-9
    KC=0
```

```
   DO 25 K=1,IN-1
   NC=NC+10
   VS=0.
   DV=0.

   DO 35 L=NC,NC+9
35  VS= VS+V(L)
   VA=VS/10.

   DO 45 L=NC,NC+9
45  DV= DV+(V(L)-VA)**2
   SIG3=(ABS(1./9.*DV))**.5*2.

   DO 54 L=NC,NC+9
   DEV= ABS(VA-V(L))
   IF (DEV.LT.SIG3) THEN
    KC=KC+1
    VN(KC)=V(L)
    TN(KC)=T(L)
    EX1N(KC)=EX1(L)
    EX2N(KC)=EX2(L)
    KENN(KC)=KEN(L)
   ENDIF
54  CONTINUE
25  CONTINUE
   DO 99 KK=1,KC
    V(KK)=VN(KK)
    T(KK)=TN(KK)
    EX1(KK)=EX1N(KK)
    EX2(KK)=EX2N(KK)
99   KEN(KK)=KENN(KK)
   NP=KC
   RETURN

   END


   SUBROUTINE SORT (F1,F2,F3,NP,F4,KEN)
   DIMENSION F1(NP),F2(NP),F3(NP),F4(NP),KEN(NP)

   IS=NP/2

100 DO 10 J=1,IS
   DO 20 I=J,NP-IS
   K=I
   NT=KEN(I+IS)
   T1=F1(I+IS)
   T2=F2(I+IS)
   T3=F3(I+IS)
   T4=F4(I+IS)

30  IF (K.GE.J) THEN
     IF(NT.GE.KEN(K)) GO TO 60
```

```
      KEN(K+IS)=KEN(K)
      F1(K+IS) =F1(K)
      F2(K+IS) =F2(K)
      F3(K+IS) =F3(K)
      F4(K+IS) =F4(K)
      K=K-IS
      GOTO 30
    ENDIF

60  KEN(K+IS)=NT
    F1(K+IS)=T1
    F2(K+IS)=T2
    F3(K+IS)=T3
    F4(K+IS)=T4
    K=K-IS
20  CONTINUE
10  CONTINUE

    IS=IS/2
    IF(IS.GE.1) GOTO 100
    RETURN
    END

    SUBROUTINE GROUP(NP,F1,F2,F3,F4,KEN,NW,F1N,F2N,F3N,F4N,KENN)
    DIMENSION F1(NP),F2(NP),F3(NP),F4(NP),KEN(NP),F1N(NP/5)
   *,F2N(NP/5),F3N(NP/5),F4N(NP/5),KENN(NP/5)

    NF=0
    LL=0
    II=0

    LW=25
    NW=1200/LW
    IP=LW/2

75  II=II+1
    IF(KEN(II).LE.IP) THEN
      GOTO 75
    ENDIF
    II=II-1

    DO 60 LL=1,NW-1
    F1S=0
    F2S=0
    F3S=0
    F4S=0
    J=0

40  IP=IP+LW

30  II=II+1
    IF(II.GT.NP) GOTO 67
    IF (KEN(II).LE.IP) THEN
```

```
      J=J+1
      GOTO 30
    ELSE
      IF(J.EQ.0) THEN
        NF=NF+1
        KENN(LL)=IP-LW/2

        GOTO 60
      ENDIF
    ENDIF

67  II=II-1
    IT=II-J+1

    DO 80 K=IT,II
      F1S=F1S+F1(K)
      F2S=F2S+F2(K)
      F3S=F3S+F3(K)
80    F4S=F4S+F4(K)

    F1N(LL)=F1S/REAL(J)
    F2N(LL)=F2S/REAL(J)
    F3N(LL)=F3S/REAL(J)
    F4N(LL)=F4S/REAL(J)
    KENN(LL)=IP-LW/2



    IF(NF.GT.0) THEN
      IB=LL-NF
      IF(IB.EQ.0) THEN
        WRITE(*,*)'DATA TOO SPARCE'

      ENDIF

      SLP1=(F1N(LL)-F1N(IB-1))/REAL(LW)/REAL(NF+1)
      SLP2=(F2N(LL)-F2N(IB-1))/REAL(LW)/REAL(NF+1)
      SLP3=(F3N(LL)-F3N(IB-1))/REAL(LW)/REAL(NF+1)
      SLP4=(F4N(LL)-F4N(IB-1))/REAL(LW)/REAL(NF+1)

      DO 90 K=IB,LL-1
      F1N(K)=F1N(K-1)+SLP1*REAL(LW)
      F2N(K)=F2N(K-1)+SLP2*REAL(LW)
      F3N(K)=F3N(K-1)+SLP3*REAL(LW)
90    F4N(K)=F4N(K-1)+SLP4*REAL(LW)
      NF=0
    ENDIF

60  CONTINUE


    JJ=0
    F1S=0
```

```
      F2S=0
      F3S=0
      F4S=0

      KENN(NW)=1200
      DO 111 NN=1,NP
      IF (KEN(NN).LE.LW/2.OR.KEN(NN).GE.1200-LW/2) THEN
        F1S=F1S+F1(NN)
        F2S=F2S+F2(NN)
        F3S=F3S+F3(NN)
        F4S=F4S+F4(NN)
        JJ=JJ+1
      ENDIF
  111 CONTINUE

      F1N(NW)=F1S/REAL(JJ)
      F2N(NW)=F2S/REAL(JJ)
      F3N(NW)=F3S/REAL(JJ)
      F4N(NW)=F4S/REAL(JJ)

      RETURN
      END

      SUBROUTINE FORIER(N,M,TIME,X,KT,AZERO,A,B,XSIN,XCOS,LLX,FRQ)
      DIMENSION X(N),KT(N),A(M),B(M),XSIN(N),XCOS(N)
      PI=3.1416
      SUMZ=0.0
      DO 100 I=1,N
  100 SUMZ=SUMZ+X(I)
      AZERO=SUMZ/REAL(N)
      DO 300 II=1,M
      SUMS=0.0
      SUMC=0.0
      DO 200 I=1,N
      THETA=2.*PI*REAL(KT(I))*REAL(II)/TIME
      XCOS(I)=X(I)*COS(THETA)
      XSIN(I)=X(I)*SIN(THETA)
      SUMS=SUMS+XSIN(I)
      SUMC=SUMC+XCOS(I)
  200 CONTINUE
      A(II)=2.*SUMC/REAL(N)
      B(II)=2.*SUMS/REAL(N)

C*****************************************************************
C  LLX=1 MEANS THAT HEAT FLUX DATA IS BEING DECOMPOSED.  THIS   *
C  HEAT FLUX DATA NEEDS TO  BE ADJUSTED DUE TO THE RC FILTER    *
C  THAT WAS CONNECTED TO THE AMPLIFIER.  THE FILTER HAS A TIME  *
C  CONSTANT, FRC, OF 200 HZ.  PHASE AND AMPLITUDE WERE ADJUSTED *
C  ACCORDINGLY.                                                 *
C*****************************************************************

      IF (LLX.EQ.1) THEN
        FRC=200
```

```
      FRQ=REAL(N)*FRQ
      ZO=SQRT(A(II)**2+B(II)**2)
      PO= ATAN(B(II)/A(II))
      IF (A(II).LT.0..AND.B(II).GT.0.) THEN
        PO=PO+PI
      ENDIF

      IF (A(II).LT.0..AND.B(II).LT.0.) THEN
        PO=PO-PI
      ENDIF

      ZI= SQRT(1.+ (FRQ/FRC)**2)*ZO
      PPI= PO+ ATAN(FRQ/FRC)
      A(II)= ZI*COS(PPI)
      B(II)= ZI*SIN(PPI)
    ENDIF

300  CONTINUE
    RETURN
    END

    SUBROUTINE CONVRT(KX1,KX2,NW,EX1,EX2,CH,BARO,HFA)
    DIMENSION EX1(NW),EX2(NW),CH(2)
    CHARACTER*12 CH

    JJ=1
    GOTO (10,20,30,40) KX1

    CH(JJ)='VOLTS'
    GOTO 100

  5  JJ=2
    GOTO (10,20,30,40) KX2

    CH(JJ)='VOLTS'
    GOTO 100

 10  CH(JJ)='PRESSURE'

    CC=335.12574+BARO*14.696/29.92
    DO 15 I=1,NW
    IF(JJ.EQ.2) THEN
     EX2(I)= (2.59528*ABS(EX2(I))**2.+60.61284*EX2(I)+CC)*6.895
    ELSE
     EX1(I)= (2.59528*ABS(EX1(I))**2.+60.61284*EX1(I)+CC)*6.895
    ENDIF
 15  CONTINUE
    GOTO 100

 20  CH(JJ)='HEAT FLUX'
    DO 25 I=1,NW
    IF(JJ.EQ.2) THEN
     EX2(I)=(-1./(.201*10.**(-6)))*EX2(I)*(3.154/HFA)
```

```
      ELSE
       EX1(I)=(-1./(.201*10.**(-6)))*EX1(I)*(3.154/HFA)
      ENDIF
25    CONTINUE
      GOTO 100

30    CH(JJ)='TEMP (THRM)'
      DO 35 I=1,NW
      IF(JJ.EQ.2) THEN
       EX2(I)= EX2(I)*17.022525+EX2(I)**2*(-.2209724)+
     *   EX2(I)**3*(5.48093E-3)+ EX2(I)**4*(-5.76699E-5)
      ELSE
       EX1(I)= EX1(I)*17.022525+EX1(I)**2*(-.2209724)+
     *   EX1(I)**3*(5.48093E-3)+ EX1(I)**4*(-5.76699E-5)
      ENDIF
35    CONTINUE
      GOTO 100

40    CH(JJ)='TEMP (RTD)'
      DO 45 I=1,NW
      IF(JJ.EQ.2) THEN
       EX2(I)=5./9.*(13.13337*EX2(I))-160./9.
      ELSE
       EX1(I)=5./9.*(13.13337*EX1(I))-160./9.
      ENDIF
45    CONTINUE



100   IF (JJ.EQ.1) GOTO 5
      RETURN
      END

      FUNCTION CURV(POS,A0,A,B,M,X)
      DIMENSION A(M),B(M),X(M)
      CURV=0

      DO 20 I=1,M

      X(I)=A(I)*COS(REAL(I)*(6.263185*POS))
     * + B(I)*SIN(REAL(I)*(6.263185*POS))

20    CURV=CURV+X(I)
      CURV=CURV+A0
      RETURN
      CONTINUE
      END
```

A.2 Complex Nusselt Number and Phase Shift Program, "NUC3"

```
C*************************************************************************
C                                                                        *
C  THIS PROGRAM USES THE *.COF GENERATED BY SMOOTHY.FOR AND              *
C  DETERMINES THE COMPLEX NUSSELT NUMBER AND THE CORRESPONDING*
C  PHASE SHIFT BETWEEN HEAT FLUX AND GAS-WALL TEMPERATURE                *
C  DIFFERENCE FOR THE FIRST FIVE HARMONICS.                              *
C            By William A. Grassmyer                                     *
C                                                                        *
C*************************************************************************

    DIMENSION V(4000),P(4000),Q(4000),TC(4000),TW(4000),DT(4000)
    *,DTC(4000),DTW(4000),DDT(4000),A(50),B(50),A1(50),B1(50),
    *A2(50),B2(50),A3(50),B3(50),A4(50),B4(50),AV1(50),AV2(50),
    *BV1(50),BV2(50),XX(50),X(50),A5(50),B5(50),ZQ(50),ZT(50),
    *ZH(50),PQ(50),PT(50),DP(50),DPD(50),CNUR(50),CNUI(50)

    CHARACTER OUT*7,VOLT*3,FL*4,PH*3,D*12


 83 M=2
    CP=1005.
    DEN=1.141
    DK= .0280

    PI=3.14159
    DH=.04445
    QB=-1000000.
    QS=1000000.
    TB=-100000.
    TS=100000.
    DTB=-100000.
    DTS=10000.


    WRITE(*,*)
    WRITE(*,*)'INPUT THE VOLTAGE OF RUN(EX 050):'
    READ(*,'(A3)') VOLT

    WRITE(*,*)
    WRITE(*,*)'INPUT HIGH OR LOWB:'
    READ(*,'(A4)') FL
    WRITE(*,*)
    OUT=VOLT//FL
    WRITE(*,*) OUT

517  FORMAT(A7)

    WRITE(*,*)
    WRITE(*,*) 'PHASE ANGLE (EX. 045):'

    READ(*,'(A3)') PH
```

```
      OPEN(UNIT=8,FILE='a:\COEF\'//PH//'\'//OUT//'.COF',
     *STATUS='UNKNOWN')

      OPEN(UNIT=94,FILE='a:\NUC\'//PH//'\'//OUT//'.NUC',
     *STATUS='UNKNOWN')

      READ(8,'(/,/,/,/,/,/,/,/,/,/,/,/,/,/,/,/)')

      READ(8,*) JJ,AV10,A01,A02

      WRITE(*,*) JJ,AV10,A01,A02

      DO 30 I=1,2

30    READ(8,*) JJ,AV1(I),BV1(I),A1(I),B1(I),A2(I),B2(I)

      READ(8,*)
      READ(8,*)
      READ(8,*)

      READ(8,*)
      READ(8,'(A12,F7.4)') D,P1

      READ(8,'(/,/,/,/,/,/,/,/,/,/)')


      READ(8,*) JJ,AV20,A03,A04


      DO 40 I=1,5

40    READ (8,*) JJ,AV2(I),BV2(I),A3(I),B3(I),A4(I),B4(I)

      READ(8,*)
      READ(8,'(A12,F7.4)') D,P2

      A0=(AV10+AV20)/2.

      DO 50 I=1,M
        A05=A03-A04
        A5(I)=A3(I)-A4(I)
        B5(I)=B3(I)-B4(I)

        A(I)=(AV1(I)+AV2(I))/2.
50    B(I)=(BV1(I)+BV2(I))/2.



      PERA=(P1+P2)/2.
      W=1./PERA
      PEW=0.
```

```
      DO 12 I=1,1800
      POS=REAL(I)/1800.
      TIM=POS*PERA

      V(I)= CURV(POS,A0,A,B,M,XX)
      P(I)= CURV(POS,A01,A1,B1,M,XX)
      Q(I)= CURV(POS,A02,A2,B2,M,XX)
      TC(I)= CURV(POS,A03,A3,B3,M,XX)
      TW(I)= CURV(POS,A04,A4,B4,M,XX)
      DT(I)=TC(I)-TW(I)


      IF(TC(I).GT.TB) THEN
       TB=TC(I)
      ENDIF

      IF(TC(I).LT.TS) THEN
       TS=TC(I)
      ENDIF

      IF(Q(I).GT.QB)  THEN
       QB=Q(I)
       MQ=I
      ENDIF

      IF(Q(I).LT.QS)  THEN
       QS=Q(I)
       NQ=I
      ENDIF

      IF(DT(I).GT.DTB) THEN
       DTB=DT(I)
       MDT=I
      ENDIF

      IF(DT(I).LT.DTS) THEN
       DTS=DT(I)
       NDT=I
      ENDIF
   12 CONTINUE

      QMAX=REAL(MQ)/1800.*360.
      QMIN=REAL(NQ)/1800.*360.
      DTMX=REAL(MDT)/1800.*360.
      DTMN=REAL(NDT)/1800.*360.
      PSMX=DTMX-QMAX
      PSMN=DTMN-QMIN
      PEW=PEW/1800.

      REW=W*DH**2/4./(1.566*10.**(-5))
      PR =.7
      PEW=REW*PR
```

```
      WRITE(94,'(/,/)')
      WRITE(94,*)'FREQ= ',W
      WRITE(94,*)'PEW = ',PEW
      WRITE(94,25) QB,QMAX,QS,QMIN,DTB,DTMX,DTS,DTMN
      WRITE(94,26) PSMX,PSMN


   25  FORMAT(/,2X,'QMAX =',F9.3,' AT ',F6.2,' DEG',/,2X,'QMIN =',
     *F9.3,' AT ',F6.2,' DEG',/,2X,'DTMAX=',F9.3,' AT ',F6.2,' DEG'
     *,/,2X,'DTMIN=',F9.3,' AT ',F6.2,' DEG')

   26  FORMAT(/,/,2X,'PHASE SHIFT(MAX)= ',F7.2,/,2X,
     *'PHASE SHIFT(MIN)= ',F7.2)

C**************HARMONIC ANALYSIS OF Q AND DT**********************


      WRITE(94,*)' HARMONIC   PS(DEG)     NUr      NUi     NUC'

      DO 70 I=1,M

       IF(A5(I).EQ.0.) THEN
        A5(I)= 1*10.**(-4)
        WRITE(94,*)'ERROR'
       ENDIF


      ZQ(I)= SQRT(A2(I)**2+B2(I)**2)
      PQ(I)= ATAN(B2(I)/A2(I))
      IF(A2(I).LT.0..AND.B2(I).GT.0.) THEN
        PQ(I)=PQ(I)+PI
      ENDIF
      IF(A2(I).LT.0..AND.B2(I).LT.0.) THEN
        PQ(I)=PQ(I)-PI
      ENDIF


      ZT(I)= SQRT(A5(I)**2+B5(I)**2)
      PT(I)= ATAN(B5(I)/A5(I))

      IF(A5(I).LT.0..AND.B5(I).GT.0.) THEN
        PT(I)=PT(I)+PI
      ENDIF
      IF(A5(I).LT.0..AND.B5(I).LT.0.) THEN
        PT(I)=PT(I)-PI
      ENDIF


      DP(I)= (PQ(I)-PT(I))
      IF(DP(I).LT.-PI) THEN
       DP(I)=2.*PI+DP(I)
      ENDIF
```

```
      IF(DP(I).GT.PI) THEN
        DP(I)=DP(I)-2.*PI
      ENDIF


      ZH(I)= ZQ(I)/ZT(I)*DH/DK
      CNUR(I)= ZH(I)*COS(DP(I))
      CNUI(I)= ZH(I)*SIN(DP(I))
      DPD(I)=360./(2.*PI)*DP(I)
   70 WRITE(94,33) I,DPD(I),CNUR(I),CNUI(I),ZH(I)

   33 FORMAT(6X,I2,4F10.3)


  701 WRITE(*,485)
  485 FORMAT(/,/,5X,'WANT TO RUN AGAIN?',/,9X,'1) YES',/,9X,'2) NO',/)
      READ(*,*) NNN
      IF(NNN.EQ.1) GOTO 83


      END
C*****************************************************************

      FUNCTION CURV(POS,A0,A,B,M,X)
      DIMENSION A(M),B(M),X(M)
      PI=3.141593
      CURV=0

      DO 20 I=1,M

      X(I)=A(I)*COS(REAL(I)*(2*PI*POS))
     * + B(I)*SIN(REAL(I)*(2*PI*POS))

   20 CURV=CURV+X(I)
      CURV=CURV+A0
      RETURN
      END


      FUNCTION DCRV(POS,A0,A,B,M,DX,W)
      DIMENSION A(M),B(M),DX(M)
      PI=3.141593
      DCRV=0

      DO 20 I=1,M

      DX(I)= -A(I)*REAL(I)*2.*PI*W*SIN(REAL(I)*(2.*PI*POS))+
     *  B(I)*REAL(I)*2.*PI*W*COS(REAL(I)*(2.*PI*POS))

   20 DCRV=DCRV+DX(I)
      RETURN
      END
```

Appendix B

Baseline Data

Run #	Ψ	Freq. (Hz)	Pe_ω	r_p	Nu_c (1st)	ΔΦ (1st)	Nu_c (2nd)	ΔΦ (2nd)
T003R10 T001R45	0	1.2	26.7	1.73	79.8	-77.7	102.6	-66.0
T003R11 T001R47	0	2.8	62.5	1.72	117.3	-61.5	339.0	-42.4
T003R12 T001R49	0	3.3	72.2	1.74	191.5	-66.1	289.1	-68.7
T003R13 T001R51	0	4.9	107.8	1.75	207.0	-77.0	431.9	-52.3
T003R14 T001R53	0	6.0	131.6	1.78	249.6	-55.2	647.4	-65.4
T003R15 T001R55	0	6.8	137.7	1.74	281.0	-75.0	703.2	-66.9
T003R16 T001R57	45	1.3	28.0	1.65	109.5	-29.5	263.6	-44.8
T003R17 T001R59	45	2.8	61.2	1.69	161.3	-11.5	310.7	-10.4
T003R18 T001R61	45	3.4	74.5	1.69	199.9	-8.3	301.0	-21.2
T003R20 T001R63	45	4.6	98.1	1.68	214.6	7.4	497.8	-25.6
T003R24 T001R65	45	5.4	119.7	1.70	231.4	11.4	515.7	-50.7
T003R26	45	5.9	129.5	1.71	292.0	7.2	785.0	-99.5

T001R67								
T003R28 T001R69	90	1.4	31.8	1.50	117.2	-20.3	129.5	-63.8
T003R29 T001R71	90	2.7	60.4	1.46	224.4	-17.4	329.4	-24.3
T003R30 T001R73	90	3.6	80.3	1.46	277.8	-0.3	426.2	-12.3
T003R31 T001R75	90	4.9	108.7	1.50	308.0	-10.7	739.7	-96.9
T003R32 T001R77	90	5.3	117.7	1.58	318.4	33.2	778.4	-76.1
T003R33 T001R79	90	6.4	141.3	1.63	354.3	42.1	853.9	-22.5
T003R34 T001R81	135	1.4	30.0	1.14	175.8	-24.4	218.5	-87.5
T003R35 T001R83	135	2.7	58.7	1.14	284.7	-5.0	286.3	-33.6
T003R36 T001R85	135	3.4	74.8	1.14	292.5	9.7	450.7	-14.5
T001R86 T001R87	135	4.6	98.1	1.15	376.2	11.6	517.8	-39.7
T001R88 T001R89	135	5.5	121.7	1.14	397.8	4.7	674.6	-23.6
T001R90 T001R91	135	6.2	137.4	1.20	426.6	30.5	897.4	-15.7

References

1. Aerometrics Incorporated, Sales Brochure "Aerometrics Doppler Signal Analyzer."

2. Aerometrics Incorporated, Sales Brochure "Aerometrics Laser Doppler Velocimeter Systems."

3. Dean, C.E., 1993 "Establishing Baseline Data for an Experimental Apparatus that Measures Heat Transfer Under Conditions of Oscillating Pressure and Flow," M.S. Thesis, Dept. of Mesh. Eng., MIT.

4. Faulkner, H.B., 1983, "An Investigation of Instantaneous Heat Transfer During Compression and Expansion in Reciprocating Gas Handling Equipment," Ph.D. Thesis, Dept. of Mech. Eng., MIT.

5. Friedlander, S.K., *Smoke, Dust and Haze-Fundamentals of Aerosol Behavior*, John Wiley & Sons, New York, 1977, pp.42-44.

6. Fuchs, N.A., *The Mechanics of Aerosols*, The MacMillan Company, New York, 1964, pp. 110-113, 250-257.

7. Gedeon, D., 1986, "Mean-Parameter Modelling of Oscillating Flow," Journal of Heat Transfer, Vol. 108, No. 3, pp. 513-518, August.

8. Grassmyer, W.A., 1994, "Experiments in Heat Transfer Under Conditions of Oscillating Pressure and Flow," M.S. Thesis, Dept. of Mech. Eng., MIT.

9. Hesketh, H.E., *Fine Particles in Gaseous MediaI*, Ann Arbor Science Publisher Inc. Michigan, 1977, pp. 93-94.

10. Ho, Y., 1991, "Experimental Investigation of Heat Transfer With Combined Oscillating Pressure and Oscillating Flow," M.S. Thesis, Dept. of Mech. Eng., MIT.

11. Jeong, E.S., 1991, "Heat Transfer with Oscillating Pressure in Reciprocating machinery Flow," Ph.D. Thesis, Dept. of Mech. Eng., MIT.

12. Kornhauser, A.A., and Smith, J.L. Jr., 1987, "A Comparison of Cylinder Heat Transfer Expressions Based on Prediction of Gas Spring Hysteresis Loss," Fluid Flow and Heat Transfer in Reciprocating Machinery, American Society of Mechanical Engineers, pp. 89-96.

13. Kornhauser, A.A., and Smith, J.L. Jr., 1988, "Application of a Complex Nusselt Number to Heat Transfer During Compression and Expansion," On Flows in Internal Combustion Engine-IV, American Society of Mechanical Engineers, pp. 1-8.

14. Kornhauser, A.A., and Smith, J.L. Jr., 1989, "Heat Transfer with Oscillating Pressure and Oscillating Flow," Proceedings of the 24th Intersociety Energy Conversion Engineering Conference, pp. 2743-2753.

15. Kornhauser, A.A., 1991 "Gas-Wall Heat Transfer During Compression and Expansion," Sc.D. Thesis, Dept. of Mech Eng., MIT.

16. Kurzweg, U.H., 1985, "Enhanced Heat Conduction in Fluids Subjected to Sinusoidal Oscillations," Journal of Heat Transfer, Vol 107, pp. 495-462.

17. Lee, K.P., 1983, "A Simplistic Model of Cyclic Heat Transfer Phenomenon Closed Spaces," Proceedings of the 18th Intersociety Energy Conversion Engineering Conference, pp. 720-723.

18. Licht, W., *Air Pollution Control Engineering*, Dekker, NY, 1980, pp.152-154, 196-198.

19. Lienhard, J.H., *A Heat Transfer Textbook*, Prentice-Hall, Englewood Cliffs, NJ, 1987.

20. Martini, W.R., "Stirling Engine Design Manual," Martini Engineering, National Aeronatics and Space Administration, Lewis Research Center Under Grant NSG-3194, pp. 1-41.

21. Overbye, V.D., Bennethum, J.E., Uychara, O.A., and Myers, P.S. 1961, "Unsteady Heat Transfer in Engines," SAE Transaction, Vol 69, pp. 461-493.

22. Pfriem, H., 1943, "Periodic Heat Transfer at Small Pressure Fluctuations," NACA-TM-1048, National Advisory Committee for Aeronautics, (Translated from Forschung auf dem Gebiete des Ingenierwesens, Vol 11, No. 2, 1940, pp. 67-75).

23. Schlichting, H., *Boundary Layer Theory*, McGraw-Hill, New York, 1979, pp. 436-439.

24. Shaw, D. T., *Fundamentals of Aerosol Science*, John Wiley & Sons, New York, 1978, pp. 29-31, 85-88.

25. Simon, T.W., and Seume, J.R., 1988, "A Survey of Oscillating Flow in Stirling Engine Heat Exchangers," NASA-CR-182108.

26. Sullivan, J.P., 1973 "Experimental Inestigation of Vortex Rings and Helicopter Rotor Waves using a Laser Doppler Velocimeter" Sc.D. Thesis, Dept of Aero and Astro., MIT.

27. Tzrianis, A.K., 1992, "Temperature, Heat Flux, and Velocity Measurements in Oscillating Flows and Pressure Variations," M.S. Thesis, Dept. of Mech. Eng., MIT.

28. Walker, G., *Stirling Engines*, Oxford University Press, New York, NY, 1980.

29. West, C.D., *Principles and Applications of Stirling Engines*, Van Nostrand Reinhold Company, New York, NY, 1986.

30. White, F.M., *Viscous Fluid Flow*, McGraw-Hill, New York, 1991, pp135-136.